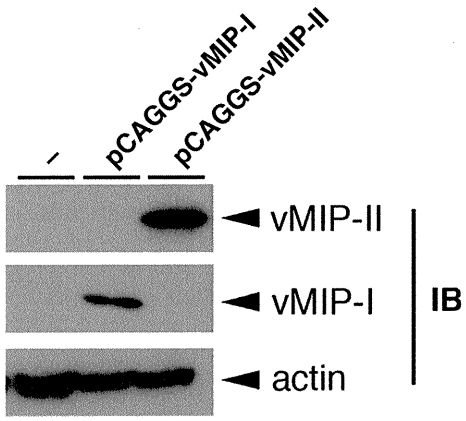

Fig. 1. Cross reactivity between anti-vMIP-I and anti-vMIP-II MAb. 293 T cells were transfected with either 2 μg of pCAGGS- vMIP-I or 2 μg of pCAGGS-vMIP-II plasmids. Forty-eight hours after transfection, the cells were harvested and expression of vMIP-I or vMIP-II was tested by Western blot analysis using the anti-vMIP-I or -vMIP-II MAb, respectively. Actin was also probed with anti-actin monoclonal Ab as a loading control.

obtained from the American Type Culture Collection (ATCC) (Manassas, VA). These cells were grown in RPMI 1640 (Nakalai Tesque, Inc., Kyoto, Japan) supplemented with 10 IU/ml penicillin G, 10 μg/ml streptomycin, 10% heat-inactivated fetal bovine serum (FBS) (HyClone, Logan, UT) in a 5% CO_2 atmosphere. In addition, 293 T and 293/EBNA (Clontech) cells were grown in Dulbecco's modified Eagle's medium (DMEM) (Nakalai Tesque, Inc.) supplemented with 10 IU/ml penicillin G, and 10 μg/ml streptomycin, 10% FBS, and 200 mM L-glutamine.

Plasmids

In order to express vMIP-I and vMIP-II, the ORFs were cloned into the pCAGGS eukaryotic expression vector, and pCAGGS-vMIP-I and pCAGGS-vMIP-II were established. The plasmid vector, pCAGGS was kindly provided by Dr. J. Miyazaki of Osaka University (Niwa et al., 1991). Briefly, fragments including vMIP-I and vMIP-II ORFs were amplified by PCR using the following primer sets: vMIP-I-Met (5′-CGGTACCGAATTCTCCAGATGGCC-3′) and vMIP-I-Ter (5′-ACTCGAGAATTCTACTTGTCATCGTCGTCCTTGTAGTCGGAAGCTATGGCAGGCAG-3′); and vMIP-II-Met (5′-AGGTACCGAATTCAGTTATGGACACCAAGGGC-3′) and vMIP-II-Ter (5′-ACTCGAGAATTCTACTTGTCATCGTCGTCCTTGTAGTCGGAGCGAGCAGTGACTGG-3′). The PCR products were cloned into pCR2.1 (Invitrogen) and sequenced. After digestion with *Eco*RI, the fragments were ligated into the *Eco*RI site of the pCAGGS vector. Then, the DNA fragments encoding vMIP-I and vMIP-II were liberated by *Eco*RI, and were inserted into pCAGGS to generate the expression vectors pCAGGS-vMIP-I and -vMIP-II, respectively. vMIP-I (pGEX-vMIP-I) and vMIP-II (pGEX-vMIP-II) were also generated using PCR-based technology using BCBL-1 genomic DNA as a templete. The coding region, without a signal peptide, was amplified with vMIP-I-Eco (CAGAATTCGCGGGGTCACTCGTGTCG-3′), vMIP-I-Sal (CTGTCGACCGTCTAAGCTATGGCAGG-3′), vMIP-II-Eco (5′-CGGAATTCGCGTCCTGGCATAGACCG-3′), and vMIP-II-Sal (5′-GGGTCGACATTCTTCAGCGAGCAGTG-3′). The amplified vMIP-I and the vMIP-II fragments were digested with *Eco*RI and *Sal*I and inserted downstream of the GST coding of pGEX-5X-1 (GE Healthcare, Uppsala, Sweden) at the *Eco*RI and *Sal*I sites to construct pGEX-vMIP-I and pGEX-vMIP-II. To express a full-length and the deletion mutants of the GST-vMIP-I and GST-vMIP-II fusion protein, the genes for GvM1-Full, GvM1-D1, GvM1-D2,

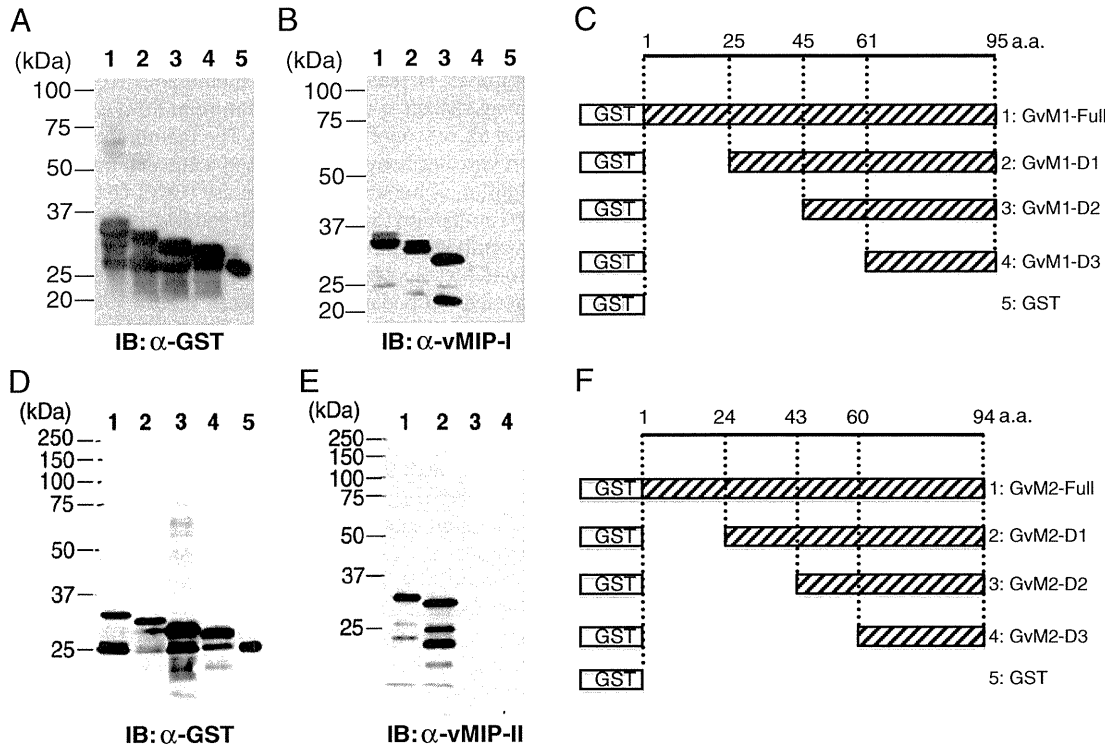

Fig. 2. Epitope mapping of the anti-vMIP-I and the anti-vMIP-II MAbs. To map the regions of vMIP-I and vMIP-II recognized by the anti-vMIP-I and anti-vMIP-II antibody, a series of GST-vMIP-I and GST-vMIP-II fusion proteins containing the individual regions of vMIP-I and vMIP-II were constructed as described in Fig. 2C and F, and the proteins were expressed in *E. coli*. The lysates of the fusion proteins, vMIP-I and vMIP-II, and its deletion mutants were immunoblotted with an anti-GST antibody (A and D) and an anti-vMIP-I (B) and an anti-vMIP-II antibody (E) to detect GST-vMIP-I or GST-vMIP-II fusion proteins. Lane 1, GvM1-Full; lane 2, GvM1-D1; lane 3, GvM1-D2; lane 4, GvM1-D3; lane 5, GvM1-D4; lan3 6, GST in Fig. 2A and B. Lane 1, GvM2-Full; lane 2, GvM2-D1; lane 3, GvM2-D2; lane 4, GvM2-D3; lane 5, GST (in D only) in Fig. 2D and E. Summary of GST-vMIP-I (C) and GST-vMIP-II (F) deletion mutants. Individual regions of vMIP-I and vMIP-II were cloned in-frame into the pGEX-5X-1 vector to generate GST-vMIP-I and GST-vMIP-II fusion proteins, respectively. The boxes at left indicate GST, and the white boxes with slashed lines indicate individual domains of vMIP-I and vMIP-II. 1, GvM1-Full(1-95a.a.); 2, GvM1-D1(25-95a.a.); 3, GvM1-D2(45-95a.a.); 4, GvM1-D3(61-95a.a.) in Fig. 2C, and 1, GvM2-Full(1-94a.a.); 2, GvM2-D1(24-94a.a.); 3, GvM2-D2(43-94a.a.); 4, GvM2-D3(60-94a.a.) in Fig. 2F.

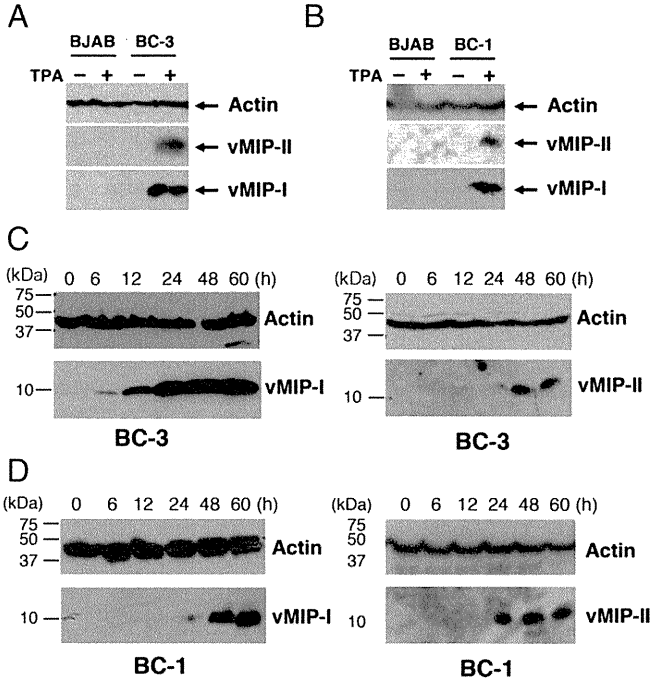

Fig. 3. Detection of vMIP-I and vMIP-II gene products in a KSHV-infected PEL cell line. BC-1 and BC-3 cells were treated with TPA for the indicated number of hours, and the whole-cell extract was prepared after the indicated time post-induction. vMIP-I and vMIP-II were detected by Western blotting and IFA with anti-vMIP-I and -vMIP-II antibodies. Western blot analysis of protein extracted from BC-3 and BJAB cells (A), and BC-1 and BJAB cells (B) with either the anti-vMIP-I or the anti-vMIP-II MAb. Arrows indicate actin, vMIP-I, and vMIP-II proteins. As expected, the estimated sizes of the vMIP-I and vMIP-II proteins, based on comparisons with the migration of molecular size markers, was around 10 kDa. Expression kinetics of vMIP-I (left panel) and vMIP-II (right panel) in TPA-treated BC-3 (C) and BC-1 (D) cells by Western blot analysis. BC-1 and BC-3 cells were harvested after 6, 12, 24, 48, and 60 h post-induction. The lysate was subjected to Western blot analysis as in (A).

GvM1-D3, GvM2-Full, GvM2-D1, GvM2-D2, and GvM2-D3 genes were generated by PCR using the following primer sets: vMIP-I-1F (5′-ATGAATTCCAGATGGCCCCCGTCCAC-3′) and vMIP-I-5R (5′-CCGTGTCGACCGTCTAAGCTATGGCAGGCAGC-3′); vMIP-I-2F (5′-ATGAATTCGCGGGGTCACTCGTGTCG-3′) and vMIP-I-5R; vMIP-I-3F (5′-ATGAATTCCCGCCCGTCCAAATTC-3′) and vMIP-I-5R; vMIP-I-4F (5′-ATGAATTCCCAAAACCCGGAGTTATTTTGC-3′) and vMIP-I-5R; vMIP-II-1F (5′-CGGAATTCGTTATGGACACCAAGGGC-3′) and vMIP-II-5R (5′-GGCAGTCGACTCTTCAGCGAGCAGTGACTG-3′); vMIP-II-2F (5′-GGGAATTCCTGGGAGCGTCCTGGCATAGAC-3′) and vMIP-II-5R; vMIP-II-3F (5′- AAGAATTCTTACCACAGGTGCTTCTGTCC-3′) and vMIP-II-5R; and vMIP-II-4F (5′-TGGAATTCAAGCCGGGTGTGATATTTTTG-3′) and vMIP-II-5R. The PCR products were cloned into pCR2.1 (Invitrogen, Carlsbad, CA) and confirmed by sequencing. The products were digested with the *Eco*RI and *Sal*I restriction enzymes and were cloned into pGEX-5X-1 (GE Healthcare). The PCR conditions for all products were as follows: 25 cycles of 94 °C for 1 min, 55 °C for 1 min, and 72 °C for 2 min in a TP480 PCR thermal cycler (Takara Shuzo, Kyoto, Japan).

Immunization and generation of monoclonal Abs against vMIP-I and vMIP-II

In mice, anti-vMIP-I and -vMIP-II antibodies were raised against the GST-vMIP-I and GST-vMIP-II fusion protein, respectively. These GST fusion proteins were purified on a glutathione-Sepharose 4B column (GE Healthcare), and the GST-vMIP-I and the GST-vMIP-II fusion proteins were conjugated to keyhole limpet hemocyanin KLH (Calbiochem. Co., La Jolla, CA). Mice were initially immunized with 250 μg each of the purified GST-vMIP-I or -II fusion protein in Freund's complete adjuvant administered to the peritoneal cavity, and 200 μg of the antigen in Freund's incomplete adjuvant were injected again 14 and 28 days after the first injection. The mice were exsanguinated 7 days after the last injection. To generate MAbs against vMIP-I and vMIP-II, hybridomas were established by fusing splenocytes from the hyperimmune mice using a nonproducing myeloma cell line, Sp-2/0-Ag14 (ATCC, Manassas, VA). After selection in medium containing hypoxanthine-aminopterin-thymidine, cells secreting MAbs were screened by immunofluorescence assays (IFA). The TPA-induced and -uninduced BCBL-1 cells were fixed in acetone and exposed to supernatants of the hybrid cells. Clones secreting antibodies reactive with TPA-stimulated BCBL-1 cells were expanded and isolated by limiting dilutions.

Transfection analysis of vMIP-I and vMIP-II

To express the vMIP-I and vMIP-II proteins, 293/EBNA cells were transfected with pCAGGS-vMIP-I and -vMIP-II plasmids using TransIT-LT1 (Mirus Bio LLC, Madison, WI). The transfected cells were incubated for 48 h in DMEM supplemented with 10% FCS. The cells were harvested and lysed with lysis buffer (0.05 M Tris-HCl [pH 8.0], 0.15 M NaCl, 0.5% sodium deoxycholate, 1% Triton X-100, 0.1% sodium-dodecyl sulfate [SDS]). The cell lysate was fractionated by electrophoresis on 16% polyacrylamide gel as described below.

Antibodies and Western blotting

The expression of vMIP-I and vMIP-II in BC-3 cells stimulated with TPA was determined with MAbs against vMIP-I and vMIP-II, respectively, as noted above. The concentration of proteins extracted from BC-3 cells was normalized using a BCA Protein Assay Kit (Thermo Fisher Scientific Inc., Rockford, IL). The samples were subjected to SDS-15% polyacrylamide gel electrophoresis under reducing conditions, and were electrophoretically transferred to PVDF membranes (Bio-Rad Laboratories, Hercules, CA). The membranes were blocked for 1 h while being shaken at room temperature in PBS containing 0.05% Tween 20 and 5% w/v nonfat skim milk. The membranes were incubated with a primary antibody and were then incubated for 1 h with an appropriate dilution of horseradish peroxidase (HRP)-conjugated goat anti-mouse IgG antibodies (Santa Cruz Biotechnologies, Santa Cruz, CA). The primary antibody against actin, anti-actin (Ab-1) mouse MAb, was purchased from Merck (Merck KGaA, Darmstadt, Germany). The bound HRP-labeled antibodies were detected with a West Pico substrate kit for horseradish peroxidase (Thermo Fisher Scientific Inc).

IFA

BC-3 cells (10^7 cells) in RPMI 1640 medium with supplements were induced with 25 ng/ml TPA (Sigma Chemical Co., St. Louis, MO). The cells were collected after 0, 4, 8, 12, 24, 48, and 60 h for analysis of the expression kinetics, and for cellular localization analysis 48 h after exposure to TPA. The cells were washed in phosphate-buffered saline (PBS), pH 7.4, and spotted on glass slides. The spots were air-dried, then fixed in ice-cold acetone for 10 min. The cells were then washed with a washing buffer (PBS supplemented with 0.1% Triton X-100) for 15 min, and incubated with either an anti-vMIP-I or an anti-vMIP-II MAb (diluted 1:100 in IFA dilution buffer [PBS containing 2% bovine serum albumin, 0.2% Tween-20, and 0.05% NaN_3]) for 1 h at 37 °C. Then, the slides were washed with the washing buffer, and incubated for 1 h at room temperature with a pre-standardized diluted fluorescein isothiocyanate (FITC)-conjugated goat anti-mouse IgG (Tago Immunologicals, Camarillo, CA). The slides were washed and stained with 4′, 6′-diamidino-2-phenylindole (DAPI) to detect nuclei and were mounted with 50% (v/v) glycerol in PBS. For formalin-fixed paraffin-embedded tissues, antigen retrievals were performed on the de-paraffined sections using citrate buffer. Alexa 488 or 568-conjugated

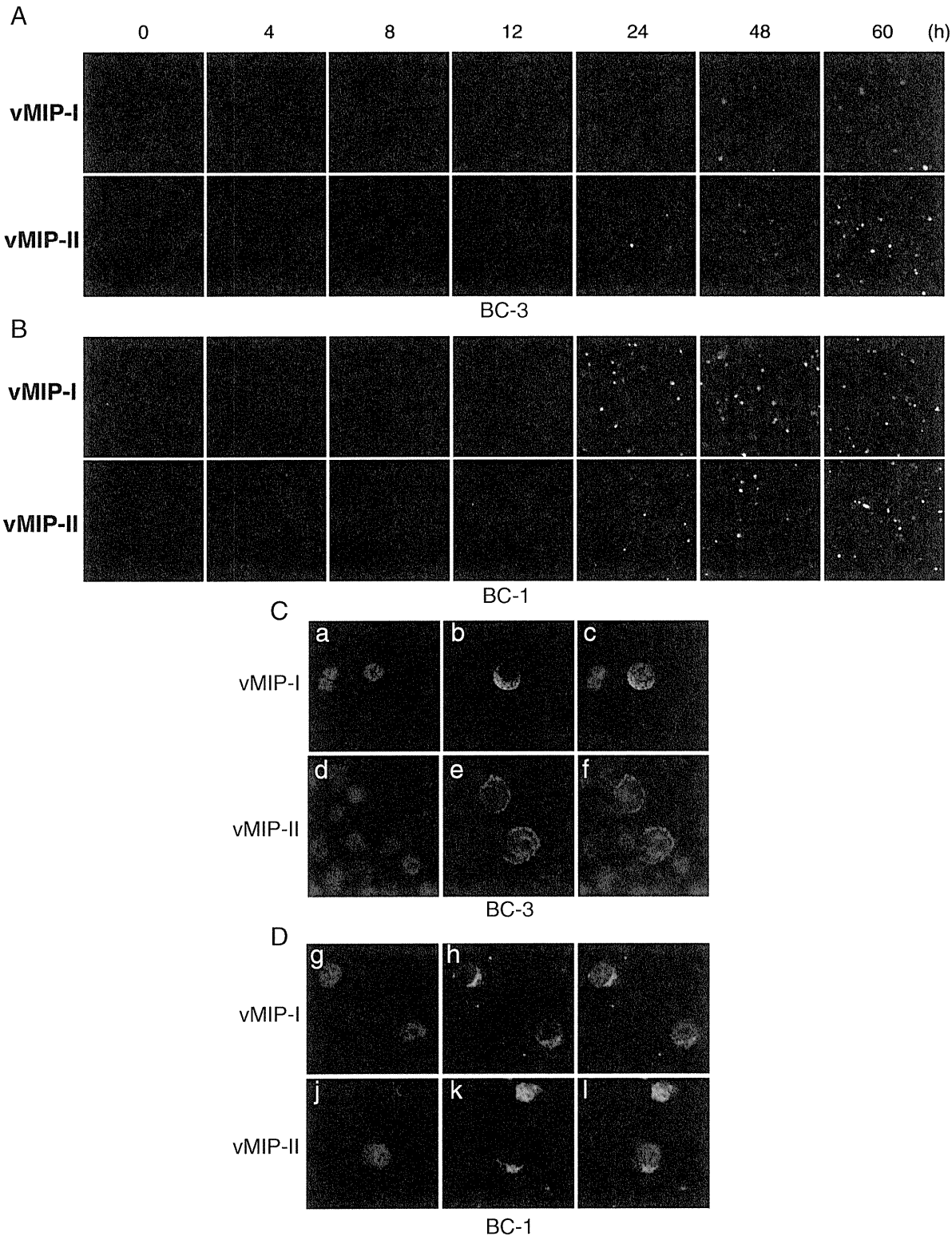

Fig. 4. Expression of vMIP-I and vMIP-II in BC-3 and BC-1 cells by IFA. After 4, 8, 12, 24, 48, and 60 h, BC-3 (A) and BC-1 (B) cells were labeled either with the anti-vMIP-I (upper) or the anti-vMIP-II (lower) MAb followed by goat anti-mouse FITC-conjugated Abs. FITC photomicrographs showing anti-vMIP-I and anti-vMIP-II immunoreactivity in BC-3 and BC-1 cells treated with TPA. (C) Cellular localization of vMIP-I and vMIP-II in BC-3 (C) and BC-1 (D) cells. The cells were stained with DAPI (a, d, g and j), and the localization of vMIP-I and vMIP-II was visualized by IFA with anti-vMIP-I or -vMIP-II MAbs (b, e, h and k); panel a and b, d and e, g and h, and j and k were merged (c, f, i and l). Fluorescence photomicrographs revealed anti-vMIP-I and -vMIP-II immunoreactivity using FITC-conjugated anti-mouse IgG MAb.

anti-mouse or rabbit antibodies (Invitrogen) were used as the secondary antibodies. Confocal microscopic analysis was performed (FV-1000, Olympus, Tokyo, Japan), and the contrast was adjusted before the images were exported as TIFF files to Adobe Photoshop.

Immunohistochemistry

Formalin-fixed paraffin-embedded tissues from KS and MCD patients, and those from an animal model of KSHV-associated solid lymphoma

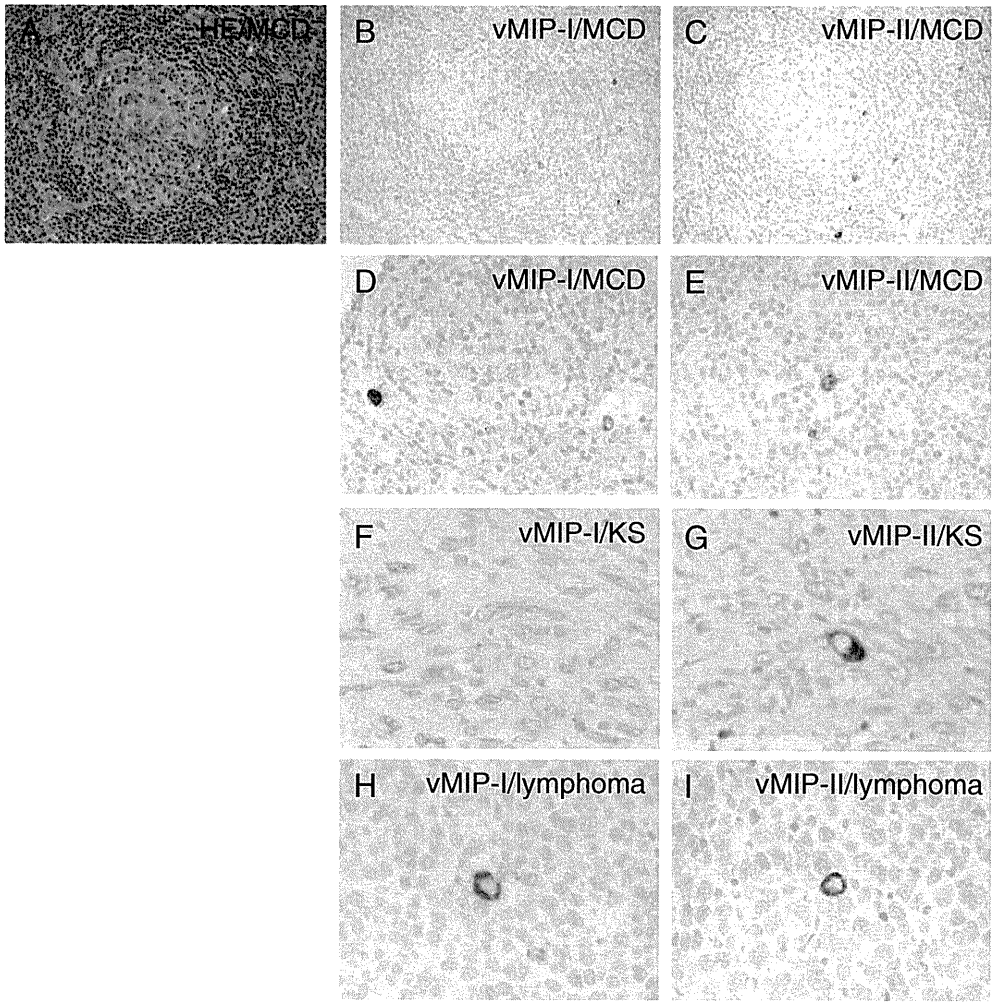

Fig. 5. Expression of vMIP proteins in KSHV-associated diseases. (A–C) Hematoxylin and eosin staining and immunohistochemistry for vMIPs in serial sections of a tissue sample from a patient with MCD. Brown stains indicate positive signals. The nucleus was counter-stained by hematoxylin. (D and E) Higher magnification view of vMIPs expression in an MCD case. Some large lymphocytes in the mantle zone were stained. (F and G) vMIP-I and vMIP-II expression in a KS sample. (H and I) Expression of vMIPs in an animal model of KSHV-associated lymphoma in SCID mice.

were sectioned and stained with hematoxylin and eosin (H&E). Immunohistochemistry of the serial sections was performed with either the anti-vMIP-I or -II MAb. For the second- and third- phase reagents used for immunostaining, a CSAII kit (DAKO, Copenhagen, Denmark) was used. An animal model of KSHV-associated solid lymphoma, which was established as described previously (Katano et al., 2000b), was also subjected to immunohistochemical analysis. Briefly, TY-1 cells were inoculated into the subcutaneous tissue of mice with severe combined immunodeficiency (SCID). One month after inoculation, lymphomas appeared in the subcutaneous region at the inoculation site. Lymphoma cells contained the KSHV genome, and expressed various viral proteins of KSHV (Katano et al., 2000b).

Table 1
Expression of vMIP-I and vMIP-II in MCD and KS tissue samples.

	KSHV proteins, (+)/total	
Cases	vMIP-I	vMIP-II
MCD	(3)/3	(3)/3
KS	(0)/5	(2)/8

Chemotaxis assays

Chemotaxis assays were performed as described previously (Nakano et al., 2003). Briefly, THP-1 cells were washed twice with chemotaxis buffer, 0.5% bovine serum albumin, 20 mM HEPES, pH 7.4, in RPMI 1640. Migration of cells was assessed in a cell culture chamber (Costar, Cambridge, MA), with the upper and lower compartments separated by a 3 μm pore size polycarbonate filter (???). The lower compartment of the chamber was filled with dilutions of vMIP-I, vMIP-II (R&D Systems, Minneapolis, MN) or with PBS alone, and/or with each 10 μg/ml anti-vMIP-I or -vMIP-II MAbs at a volume of 600 μl. The upper compartment contained 100 μl of THP-1 cell suspensions in chemotaxis buffer (10^5 cells/well). The chambers were then incubated for 4 hours at 37 °C, 5% CO_2, and spun at 300 x g, 4 °C, for 5 min. Finally, the cells from the lower compartment were counted.

Results

Specificity of the anti-vMIP-I MAb and the anti-vMIP-II MAb

In order to check specificity of the MAbs, we transfected vMIP-I and vMIP-II expression vectors (pCAGGS-vMIP-I, and -II) into 293/EBNA

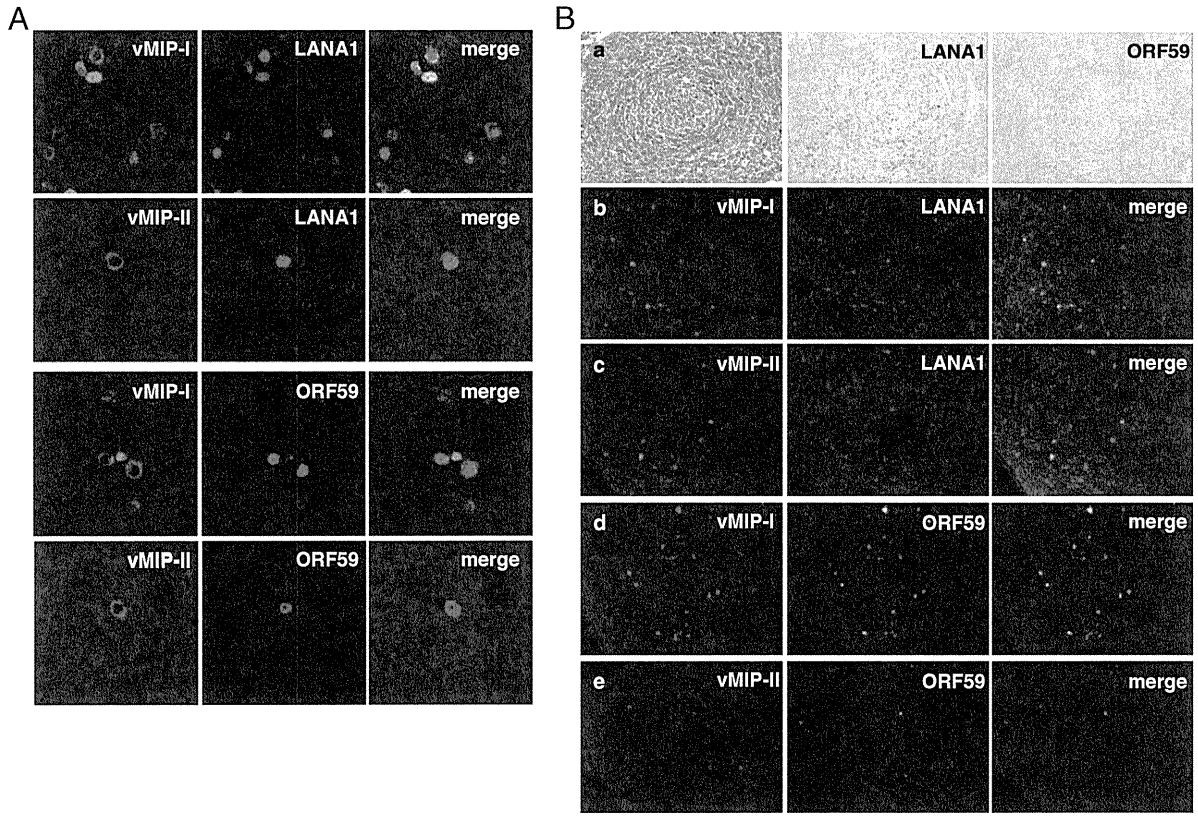

Fig. 6. (A) Expression of vMIPs. LANA1 and ORF59 in the animal model of KSHV-associated solid lymphoma by confocal microscopy. vMIPs were labeled with Alexa 488 (green). LANA1 (upper panels) and ORF59 (lower panels) were labeled with Alexa 568 (red). (B) Expression of vMIPs in MCD. (a) HE staining and immunohistochemistry of LANA1 and ORF59. (b–e) Immunofluorescence assay on MCD lesion. A germinal center is shown in the center of each panel. This case is KSHV-positive large B cell lymphoma arising in MCD.

cells, respectively. The total lysate of the transfected cells was subjected to Western blot analysis. vMIP-I and vMIP-II proteins were detected with anti-vMIP-I or vMIP-II MAbs, respectively (Fig. 1). These antibodies did not show cross-reactivity each other.

Epitope mapping of the anti-vMIP-I and anti-vMIP-II MAbs

We established hybridoma clones secreting MAbs against vMIP-I and vMIP-II, respectively. To map the regions of vMIP-I and vMIP-II where anti-vMIP-I and anti-vMIP-II antibody reacted, a series of GST-fused vMIP-I and vMIP-II deleted proteins were constructed as described in Fig. 2C and F, and used for Western blot analysis with an anti-GST antibody (Santa Cruz Biotechnology Inc), (Fig. 1A, D) and the anti-vMIP-I or the anti-vMIP-II (Fig. 1B, E) antibody, respectively. The results showed that all GST-vMIP-I and GST-vMIP-II fusion proteins interacted with the anti-GST antibody (Fig. 2A, D) and showed that GvM1-Full, GvM1-D1, and GvM1-D2 reacted with the anti-vMIP-I antibody, whereas GvM1-D3 did not (Fig. 1B), and GvM2-Full and GvM2-D1 reacted with the anti-vMIP-II antibody, whereas GvM2-D2, and GvM2-D3 did not (Fig. 2E). Thus, these results demonstrated that an anti-vMIP-I MAbs was successfully generated and suggest that the amino acid residues 61 to 95 of vMIP-I could be a major epitope reacted with the anti-vMIP-I antibody. On the other hand, the amino acid residues 24 to 42 of vMIP-II could be an epitope reacted with the anti-vMIP-II antibody.

Expression of vMIP-I and vMIP-II in the KSHV-infected PEL cell line

We tested vMIP-I and vMIP-II expression in KSHV and Epstein Barr virus (EBV) dually infected PEL cell lines (BC-1), KSHV infected PEL cell lines (BC-3) and in non-infected Burkitt's lymphoma cell line (BJAB), and detected them in TPA-stimulated BC-3 and BC-1 cells with developed antibodies, but not in BJAB cells non-stimulated BC-3 or BC-1 cells (Fig. 2A, B). In a KSHV infected PEL cells, BC-1 and BC-3, vMIP-I and vMIP-II were detected around at 10 kDa, which matches the size deduced from amino acids length (Fig. 3C, D). Actually, vMIP-I was detected from 6 hours post induction and vMIP-II was at 24 hours in BC-3 cells (Fig. 3C), and vMIP-I and vMIP-II were detected at 24 h in BC-1 cells (Fig. 3D). In the immunofluorescence microscopy, the number of vMIP-II expressing cells seemed to be more than that of vMIP-I in BC-3 cells (Fig. 4A, B). In order to analyze the cellular localization of vMIP-I and vMIP-II protein, BC-3 and BC-1 cells stimulated with TPA were doubly labeled with DAPI (Fig. 4C, a, d and D, g, j), and either the anti-vMIP-I MAb (Fig. 4C, b and D, h) or the anti-vMIP-II MAb (Fig. 4C, e and D, k). Merged images were shown in Fig. 4C, c, f, and D, i, l). The vMIP-I and the vMIP-II clearly showed cytoplasm and possibly membranes in TPA-induced BC-3 and BC-1 cells (Fig. 4C, b, e, and D, h, k).

Expression of vMIPs in KSHV-associated diseases

To know the expression of vMIPs in KSHV-associated diseases, immunohistochemistry for vMIPs was performed on pathological samples of eight KS cases, three MCD cases, and the animal model of KSHV-associated solid lymphoma (Fig. 5). Immunohistochemistry demonstrated that vMIP-I and vMIP-II were detected in some cells in the mantle zone of germinal center and the interfollicular zone in KSHV-positive MCD samples (Fig. 5A to E). Both vMIP-I and vMIP-II were detected predominantly in the cytoplasm of large lymphocytes. The numbers of positive cells varied among three MCD cases examined. On the other

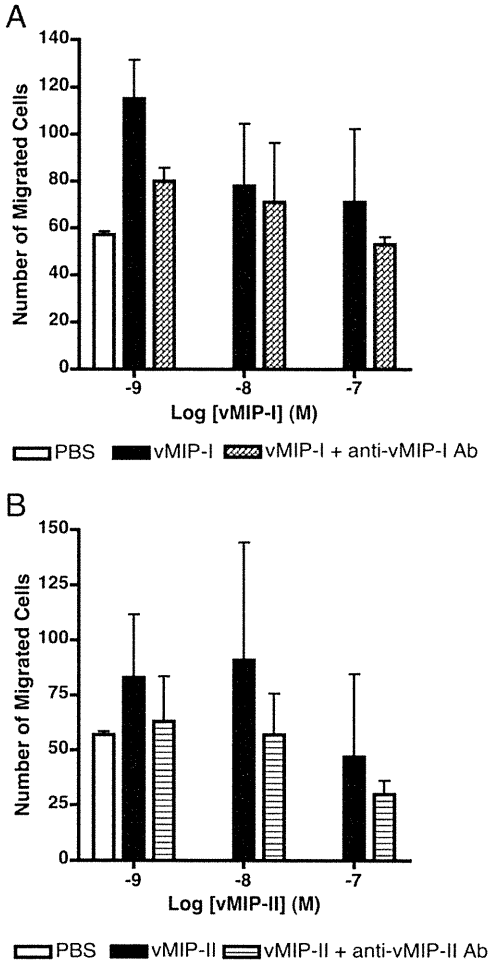

Fig. 7. Neutralizing activity of anti-vMIP-I and -vMIP-II MAbs. THP-1 cell migration in response to increased concentrations of vMIP-I and vMIP-II (1, 10, 100 nM), and the neutralizing activity of 10 μg/ml anti-vMIP-I and -vMIP-II MAbs against vMIP-I and vMIP-II were measured, as outlined in Materials and Methods, by using the transwell migration assay system. Various doses of vMIP-I and vMIP-II were tested for their ability to induce the chemotaxis of THP-1 cells. The data presented are from one experiment, and are representative of the triplicate experiments performed. The error bars indicate the standard deviations of three independent experiments.

hand, any positive signal of vMIP-I was not observed in all KS cases (Fig. 5F, G). vMIP-II was rarely detected in the cytoplasm of spindle cells in two KS cases at the nodular stage out of eight KS cases. In the samples of animal model of KSHV-associated solid lymphoma, both vMIP-I and vMIP-II were detected in the cytoplasm of a part of lymphoma cells (Fig. 5H, I). These data showed that vMIP-I and vMIP-II were expressed in cells in MCD and KSHV-associated lymphoma, but vMIP-II was rarely in KS (Table 1). To know the association of vMIPs expression with expression of other KSHV-encoded proteins, we examined immunofluorescence assay on KSHV-associated diseases. Since, all KSHV-infected cells express LANA1, vMIPs-positive cells were positive for LANA1. However, expression pattern of LANA1 showed diffuse nuclear staining in vMIPs-positive cells in the animal model of KSHV-associated solid lymphoma (Fig. 6A). Confocal microscopy revealed that vMIP-I stain showed usually cytoplasmic pattern, but rarely diffuse nuclear staining pattern *in vivo*. Almost all cells with vMIPs expression were also positive for ORF59 protein, a lytic protein of KSHV. IFA also demonstrated that vMIPs-positive cells expressed LANA1 at various levels in MCD clinical samples (Fig. 6B, a to c). A large portion of vMIPs-positive cells also expressed ORF59 protein in MCD (Fig. 6B, d, e). These data suggest that vMIPs are expressed by cells with KSHV-lytic infection in KSHV-associated MCD and lymphoma.

Neutralization of vMIP-I and vMIP-II by anti-vMIP-I and anti-vMIP-II MAbs

We examined whether the anti-vMIP-I and anti-vMIP-II MAbs could neutralize the chemoattractant of vMIP-I and vMIP-II to induce the migration of THP-1 cells. As expected, vMIP-I and vMIP-II induced migration of THP-1 cells (Fig. 7A, B), but not with PBS alone. However, anti-vMIP-I and anti-vMIP-II MAbs inhibited respective vMIP-I and vMIP-II-induced cell migration of THP-1 cells at 10 μg/ml final concentration.

Discussions

It was known that KSHV encodes three chemokine genes of the so-called viral macrophage inflammatory proteins: *vMIP-I*, *vMIP-II*, and *vMIP-III* in the genome. Analysis of the translated amino acid sequence indicate that the vMIP-I and vMIP-II gene have four conserved cysteines capable of forming two essential disulfide bonds (first cysteine and third cysteine, and second cysteine and fourth cysteine). The family of chemokines comprises CC, CXC, C, and CX_3C subfamilies. The vMIP-I and vMIP-II have four cysteines, the first two of which are found in the sequence of CC, which correspond to the CC profile. These gene products were expressed in the phase of KSHV lytic infection (Moore et al., 1996; Sun et al., 1999). Both vMIP-I and vMIP-II were expressed in a KSHV-infected cell lines, BC-3, which had been treated with TPA. Mono-specific polyclonal Abs against vMIP-I and vMIP-II have been described in previous studies that investigated the localization of vMIPs in PEL cells (Nakano et al., 2003). In the present study, we developed the respective MAbs that reacted either with KSHV vMIP-I or vMIP-II. We first applied these MAbs against KSHV vMIP-I and vMIP-II to detect KSHV-infected BC-3 and BC-1 cells by Western blotting and immunofluorescence assay. The Western blot analysis revealed that both the anti-vMIP-I and the anti-vMIP-II MAbs reacted to the 10-kDa proteins considered specific to the respective vMIP protein. The anti-vMIP-I MAb was shown to be reactive with the epitopes in the middle of the protein (sequence, PPVQILKEWYPTSPAC), and the epitope of the anti-vMIP-II MAb was shown to be reactive at the N-terminal end (sequence, LGASWHRPDKCCLGYQKRP). Further immunofluorescence analysis of the cellular localization of both vMIP-I and vMIP-II with anti-vMIP-I and anti-vMIP-II MAb showed a cytoplasmic pattern of expression in BC-3 and BC-1 cells. As the results indicated that these gene products were expressed in the cytoplasm, it might be located at the KSHV-infected BC-3 or BC-1 cells membrane prior to secretion. An investigation of the antigenic specificities of MAbs against KSHV vMIP-I and vMIP-II in MCD and KS patients has not yet been reported. Here, immunohistochemical analysis detected only vMIP-II in samples from both KS and MCD patients, but vMIP-I was not detected in KS cases: however, both vMIP-I and vMIP-II proteins were expressed in some cells in the interfollicular zone of MCD tissues. Lytic proteins of the KSHV such as K8, RTA, and ORF59 have been detected in large lymphocytes in the mantle zone of MCD cases (Dupin et al., 1999; Katano et al., 2000a). The expression of vMIPs showed a similar pattern to that of the lytic proteins in MCD tissues. In contrast, lytic protein expression, including that of vMIPs, was rare in the KS lesions (Abe et al., 2006). In the present study, we demonstrated that vMIPs were expressed in the cells expressing ORF59 protein. Thus, our data clearly indicated that the expression of vMIPs is associated with lytic infection in individual cells affected by KSHV-associated diseases. Human monocytic cell line THP-1 respond to various chemokines suggesting that they express receptors for these chemokines (Wang et al., 1993). Previous study, vMIP-I and vMIP-II were shown chemotaxis in THP-1 cells (Nakano et al., 2003). It has been reported that vMIP-I acts as a specific agonist for CC chemokine receptor 8 (CCR8) (Dairaghi et al., 1999; Endres et al., 1999) and vMIP-II shows a Ca^{2+} flux as a specific agonist for CCR3 (Boshoff et al., 1997). Our data showed anti-vMIP-I and anti-vMIP-II MAbs were able to neutralize vMIP-I- and vMIP-II-mediated chemotaxis in THP-1 cells. However, neutralizing activities

of anti-vMIP-I MAb was apparently low, even the addition of 10 μg/ml MAbs. These findings support the assumption that anti-vMIP-I and –vMIP-II MAbs-blocked chemotaxis in THP-1 cells act through binding to the certain amino acid residue of vMIP-I and vMIP-II.

In summary, MAbs developed specifically for this series were used to detect vMIP-I and vMIP-II in MCD and KS tissues, which may account for certain clinical features of MCD and KS. To gain a better understanding of these important viral genes, additional studies will be needed that focus on revealing vMIP-I and vMIP-II expression profiles during lytic infection. Taken together, these studies provide an insight into the pathogenesis of the contribution of vMIP-I and vMIP-II to the lytic induction of KSHV. These MAbs could serve as useful tools to clarify the pathogenesis of KSHV-related diseases.

Acknowledgments

This study was supported by a grant for Research on Publicly Essential Drugs and Medical Devices from the Japan Health Sciences Foundation (SAA4832), Health and Labor Sciences Research Grants (to HK, No. H23-AIDS-Ippan-002) from the Ministry of Health and by a grant from PRESTO of the Japan Science and Technology Corporation (200154023).

References

Abe, Y., Matsubara, D., Gatanaga, H., Oka, S., Kimura, S., Sasao, Y., Saitoh, K., Fujii, T., Sato, Y., Sata, T., Katano, H., 2006. Distinct expression of Kaposi's sarcoma-associated herpesvirus-encoded proteins in Kaposi's sarcoma and multicentric Castleman's disease. Pathol. Int. 56, 617–624.

Arvanitakis, L., Mesri, E.A., Nador, R.G., Said, J.W., Asch, A.S., Knowles, D.M., Cesarman, E., 1996. Establishment and characterization of a primary effusion (body cavity-based) lymphoma cell line (BC-3) harboring kaposi's sarcoma-associated herpesvirus (KSHV/HHV-8) in the absence of Epstein-Barr virus. Blood 88, 2648–2654.

Benelli, R., Barbero, A., Buffa, A., Aluigi, M.G., Masiello, L., Morbidelli, L., Ziche, M., Albini, A., Noonan, D., 2000. Distinct chemotactic and angiogenic activities of peptides derived from Kaposi's sarcoma virus encoded chemokines. Int. J. Oncol. 17, 75–81.

Boshoff, C., Endo, Y., Collins, P.D., Takeuchi, Y., Reeves, J.D., Schweickart, V.L., Siani, M.A., Sasaki, T., Williams, T.J., Gray, P.W., Moore, P.S., Chang, Y., Weiss, R.A., 1997. Angiogenic and HIV-inhibitory functions of KSHV-encoded chemokines. Science 278, 290–294.

Cesarman, E., Chang, Y., Moore, P.S., Said, J.W., Knowles, D.M., 1995. Kaposi's sarcoma-associated herpesvirus-like DNA sequences in AIDS-related body-cavity-based lymphomas. N. Engl. J. Med. 332, 1186–1191.

Chang, Y., Cesarman, E., Pessin, M.S., Lee, F., Culpepper, J., Knowles, D.M., Moore, P.S., 1994. Identification of herpesvirus-like DNA sequences in AIDS-associated Kaposi's sarcoma. Science 266, 1865–1869.

Chen, S., Bacon, K.B., Li, L., Garcia, G.E., Xia, Y., Lo, D., Thompson, D.A., Siani, M.A., Yamamoto, T., Harrison, J.K., Feng, L., 1998. In vivo inhibition of CC and CX3C chemokine-induced leukocyte infiltration and attenuation of glomerulonephritis in Wistar–Kyoto (WKY) rats by vMIP-II. J. Exp. Med. 188, 193–198.

Dairaghi, D.J., Fan, R.A., McMaster, B.E., Hanley, M.R., Schall, T.J., 1999. HHV8-encoded vMIP-I selectively engages chemokine receptor CCR8. Agonist and antagonist profiles of viral chemokines. Biol. Chem. 274, 21569–21574.

Dupin, N., Fisher, C., Kellam, P., Ariad, S., Tulliez, M., Franck, N., van Marck, E., Salmon, D., Gorin, I., Escande, J.P., Weiss, R.A., Alitalo, K., Boshoff, C., 1999. Distribution of human herpesvirus-8 latently infected cells in Kaposi's sarcoma, multicentric Castleman's disease, and primary effusion lymphoma. Proc. Natl. Acad. Sci. U. S. A. 96, 4546–4551.

Endres, M.J., Garlisi, C.G., Xiao, H., Shan, L., Hedrick, J.A., 1999. The Kaposi's sarcoma-related herpesvirus (KSHV)-encoded chemokine vMIP-I is a specific agonist for the CC chemokine receptor (CCR)8. J. Exp. Med. 189, 1993–1998.

Katano, H., Sato, Y., Kurata, T., Mori, S., Sata, T., 2000a. Expression and localization of human herpesvirus 8-encoded proteins in primary effusion lymphoma, Kaposi's sarcoma, and multicentric Castleman's disease. Virology 269, 335–344.

Katano, H., Suda, T., Morishita, Y., Yamamoto, K., Hoshino, Y., Nakamura, K., Tachikawa, N., Sata, T., Hamaguchi, H., Iwamoto, A., Mori, S., 2000b. Human herpesvirus 8-associated solid lymphomas that occur in AIDS patients take anaplastic large cell morphology. Mod. Pathol. 13, 77–85.

Kledal, T.N., Rosenkilde, M.M., Coulin, F., Simmons, G., Johnsen, A.H., Alouani, S., Power, C.A., Luttichau, H.R., Gerstoft, J., Clapham, P.R., Clark-Lewis, I., Wells, T.N., Schwartz, T.W., 1997. A broad-spectrum chemokine antagonist encoded by Kaposi's sarcoma-associated herpesvirus. Science 277, 1656–1659.

Miller, G., Heston, L., Grogan, E., Gradoville, L., Rigsby, M., Sun, R., Shedd, D., Kushnaryov, V.M., Grossberg, S., Chang, Y., 1997. Selective switch between latency and lytic replication of Kaposi's sarcoma herpesvirus and Epstein-Barr virus in dually infected body cavity lymphoma cells. J. Virol. 71, 314–324.

Moore, P.S., Boshoff, C., Weiss, R.A., Chang, Y., 1996. Molecular mimicry of human cytokine and cytokine response pathway genes by KSHV. Science 274, 1739–1744.

Nakano, K., Isegawa, Y., Zou, P., Tadagaki, K., Inagi, R., Yamanishi, K., 2003. Kaposi's sarcoma-associated herpesvirus (KSHV)-encoded vMIP-I and vMIP-II induce signal transduction and chemotaxis in monocytic cells. Arch. Virol. 148, 871–890.

Niwa, H., Yamamura, K., Miyazaki, J., 1991. Efficient selection for high-expression transfectants with a novel eukaryotic vector. Gene 108, 193–199.

Schalling, M., Ekman, M., Kaaya, E.E., Linde, A., Biberfeld, P., 1995. A role for a new herpes virus (KSHV) in different forms of Kaposi's sarcoma. Nat. Med. 1, 707–708.

Soulier, J., Grollet, L., Oksenhendler, E., Cacoub, P., Cazals-Hatem, D., Babinet, P., d'Agay, M.F., Clauvel, J.P., Raphael, M., Degos, L., et al., 1995. Kaposi's sarcoma-associated herpesvirus-like DNA sequences in multicentric Castleman's disease. Blood 86, 1276–1280.

Sun, R., Lin, S.F., Staskus, K., Gradoville, L., Grogan, E., Haase, A., Miller, G., 1999. Kinetics of Kaposi's sarcoma-associated herpesvirus gene expression. J. Virol. 73, 2232–2242.

Wang, J.M., McVicar, D.W., Oppenheim, J.J., Kelvin, D.J., 1993. Identification of RANTES receptor on human monocytic cells: competition of binding and desensitization by homologous chemotactic cytokines. J. Exp. Med. 177, 699–705.

Virus Genes
DOI 10.1007/s11262-012-0712-2

Development of a drug assay system with hepatitis C virus genome derived from a patient with acute hepatitis C

Kyoko Mori · Youki Ueda · Yasuo Ariumi · Hiromichi Dansako · Masanori Ikeda · Nobuyuki Kato

Received: 5 October 2011 / Accepted: 1 January 2012

Abstract We developed a new cell culture drug assay system (AH1R), in which genome-length hepatitis C virus (HCV) RNA (AH1 strain of genotype 1b derived from a patient with acute hepatitis C) efficiently replicates. By comparing the AH1R system with the OR6 assay system that we developed previously (O strain of genotype 1b derived from an HCV-positive blood donor), we demonstrated that the anti-HCV profiles of reagents including interferon-γ and cyclosporine A significantly differed between these assay systems. Furthermore, we found unexpectedly that rolipram, an anti-inflammatory drug, showed anti-HCV activity in the AH1R assay but not in the OR6 assay, suggesting that the anti-HCV activity of rolipram differs depending on the HCV strain. Taken together, these results suggest that the AH1R assay system is useful for the objective evaluation of anti-HCV reagents and for the discovery of different classes of anti-HCV reagents.

Keywords HCV · Acute hepatitis C · Anti-HCV drug assay system · Anti-HCV activity of rolipram

Introduction

Hepatitis C virus (HCV) infection frequently causes chronic hepatitis, which progresses to liver cirrhosis and hepatocellular carcinoma. HCV is an enveloped virus with a positive single-stranded 9.6 kb RNA genome, which encodes a large polyprotein precursor of approximately 3,000 amino acid (aa) residues [1, 2]. This polyprotein is cleaved by a combination of the host and viral proteases into at least 10 proteins in the following order: Core, envelope 1 (E1), E2, p7, non-structural 2 (NS2), NS3, NS4A, NS4B, NS5A, and NS5B [1].

Human hepatoma HuH-7 cell culture-based HCV replicon systems derived from a number of HCV strains have been widely used for various studies on HCV RNA replication [3, 4] since the first replicon system (based on the Con1 strain of genotype 1b) was developed in 1999 [5]. Genome-length HCV RNA replication systems (see Fig. 2 for details) derived from a limited number of HCV strains (H77, N, Con1, O, and JFH-1) are also sometimes used for such studies, as they are more useful than the replicon systems lacking the structural region of HCV, although the production of infectious HCV from the genome-length HCV RNA has not been demonstrated to date [3, 4]. Furthermore, these RNA replication systems have been improved enough to be suitable for the screening of anti-HCV reagents by the introduction of reporter genes such as luciferase [3, 4, 6]. We also developed an HuH-7-derived cell culture assay system (OR6) in which genome-length HCV RNA (O strain of genotype 1b derived from an HCV-positive blood donor) encoding renilla luciferase (RL) efficiently replicates [7]. Such reporter assay systems could save time and facilitate the mass screening of anti-HCV reagents, since the values of luciferase correlated well with the level of HCV RNA after treatment with anti-HCV reagents. Furthermore, OR6 assay system became more useful as a drug assay system than the HCV subgenomic replicon-based reporter assay systems developed to date [3, 4], because the older systems lack the Core-NS2 regions containing structural proteins likely to be involved in the events that take place in the HCV-infected human liver.

K. Mori · Y. Ueda · Y. Ariumi · H. Dansako · M. Ikeda · N. Kato (✉)
Department of Tumor Virology, Okayama University Graduate School of Medicine, Dentistry, and Pharmaceutical Sciences, 2-5-1 Shikata-cho, Okayama 700-8558, Japan
e-mail: nkato@md.okayama-u.ac.jp

Published online: 18 January 2012

Indeed, by the screening of preexisting drugs using the OR6 assay system, we have identified mizoribine [8], statins [9], hydroxyurea [10], and teprenone [11] as new anti-HCV drug candidates, indicating that the OR6 assay system is useful for the discovery of anti-HCV reagents.

On the other hand, we previously established for the first time an HuH-7-derived cell line (AH1) that harbors genome-length HCV RNA (AH1 strain of genotype 1b) derived from a patient with acute hepatitis C [12]. In that study, we noticed different anti-HCV profiles of interferon (IFN)-γ or cyclosporine A (CsA) between AH1 and O cells supporting genome-length HCV RNA (O strain) replication [7]. From these results, we supposed that the diverse effects of IFN-γ or CsA were attributable to the difference in HCV strains [12].

To test this assumption in detail, we first developed an AH1 strain-derived assay system (AH1R) corresponding to the OR6 assay system, and then performed a comparative analysis using AH1R and OR6 assay systems. In this article, we report that the difference in HCV strains causes the diverse effects of anti-HCV reagents, and we found unexpectedly by AH1R assay that rolipram, an anti-inflammatory drug, is an anti-HCV drug candidate.

Materials and methods

Reagents

IFN-α, IFN-γ, and CsA were purchased from Sigma-Aldrich (St. Louis, MO). Rolipram was purchased from Wako Pure Chemical Industries (Osaka, Japan).

Plasmid construction

The plasmid pAH1RN/C-5B/PL,LS,TA,$(VA)_3$ was constructed from pAH1 N/C-5B/PL,LS,TA,$(VA)_3$ encoding genome-length HCV RNA clone 2 (See Fig. 2) obtained from AH1 cells [12], by introducing a fragment of the RL gene from pORN/C-5B into the *Asc*I site before the neomycin phosphotransferase (Neo^R) gene as previously described [7].

RNA synthesis

The plasmid pAH1RN/C-5B/PL,LS,TA,$(VA)_3$ DNA was linearized by *Xba*I, and used for RNA synthesis with T7 MEGAscript (Ambion, Austin TX) as previously described [7].

Cell cultures

AH1R and OR6 cells supporting genome-length HCV RNAs were cultured in Dulbecco's modified Eagle's medium (DMEM) supplemented with 10% fetal bovine serum (FBS) and 0.3 mg/mL of G418 (Geneticin; Invitrogen, Carlsbad, CA). AH1c-cured cells, which were created by eliminating HCV RNA from AH1 cells [12] by IFN-γ treatment, were also cultured in DMEM supplemented with 10% FBS.

RNA transfection and selection of G418-resistant cells

Genome-length HCV (AH1RN/C-5B/PL,LS,TA,$(VA)_3$) RNA synthesized in vitro was transfected into AH1c cells by electroporation, and the cells were selected in the presence of G418 (0.3 mg/mL) for 3 weeks as described previously [13].

RL assay for anti-HCV reagents

To monitor the effects of anti-HCV reagents, RL assay was performed as described previously [14]. Briefly, the cells were plated onto 24-well plates (2×10^4 cells per well) in triplicate and cultured with the medium in the absence of G418 for 24 h. The cells were then treated with each reagent at several concentrations for 72 h. After treatment, the cells were subjected to a luciferase assay using the RL assay system (Promega, Madison, WI). From the assay results, the 50% effective concentration (EC_{50}) of each reagent was determined.

Quantification of HCV RNA

Quantitative reverse transcription-polymerase chain reaction (RT-PCR) analysis for HCV RNA was performed using a real-time LightCycler PCR (Roche Applied Science, Indianapolis, IN, USA) as described previously [7]. The experiments were done in triplicate.

IFN-α treatment to evaluate the assay systems

To monitor the anti-HCV effect of IFN-α on AH1R cells, 2×10^4 cells and 5×10^5 cells were plated onto 24-well plates (for luciferase assay) and 10 cm plates (for quantitative RT-PCR assay) in triplicate, respectively, and cultured for 24 h. The cells were then treated with IFN-α at final concentrations of 0, 1, 10, and 100 IU/mL for 24 h, and subjected to luciferase and quantitative RT-PCR assays as described above.

Western blot analysis

The preparation of cell lysates, sodium dodecyl sulfate–polyacrylamide gel electrophoresis, and immunoblotting analysis with a PVDF membrane were performed as described previously [13]. The antibodies used in this study were those against HCV Core (CP11 monoclonal antibody;

Institute of Immunology, Tokyo), NS5B, and E2 (generous gifts from Dr. M. Kohara, Tokyo Metropolitan Institute of Medical Science, Japan). Anti-β-actin antibody (AC-15; Sigma, St. Louis, MO, USA) was used as a control for the amount of protein loaded per lane. Immunocomplexes were detected with the Renaissance enhanced chemiluminescence assay (Perkin-Elmer Life Sciences, Boston, MA).

WST-1 cell proliferation assay

The cells were plated onto 96-well plates (1×10^3 cells per well) in triplicate and then treated with rolipram at several concentrations for 72 h. After treatment, the cells were subjected to the WST-1 cell proliferation assay (Takara Bio, Otsu, Japan) according to the manufacturer's protocol. From the assay results, the 50% cytotoxic concentration (CC_{50}) of rolipram was estimated. The selective index (SI) value of rolipram was also estimated by dividing the CC_{50} value by the EC_{50} value.

RT-PCR and sequencing

To amplify the genome-length HCV RNA, RT-PCR was performed separately in two fragments as described previously [7, 15]. Briefly, one fragment covered from 5′-untranslated region to NS3, with a final product of approximately 6.2 kb, and the other fragment covered from NS2 to NS5B, with a final product of approximately 6.1 kb. These fragments overlapped at the NS2 and NS3 regions and were used for sequence analysis of the HCV open reading frame (ORF) after cloning into pBR322MC. PrimScript (Takara Bio) and KOD-plus DNA polymerase (Toyobo, Osaka, Japan) were used for RT and PCR, respectively. The nucleotide sequences of each of the three independent clones obtained were determined using the Big Dye terminator cycle sequencing kit on an ABI PRISM 310 genetic analyzer (Applied Biosystems, Foster City, CA, USA).

Statistical analysis

Differences between AH1R and OR6 cell lines were tested using Student's t test. P values <0.05 were considered statistically significant.

Results

Development of a luciferase reporter assay system that facilitates the quantitative monitoring of genome-length HCV-AH1 RNA replication

To develop an HCV AH1 strain-derived assay system corresponding to the OR6 assay system [7], a genome-length HCV RNA encoding RL (AH1RN/C-5B/PL,LS,TA,$(VA)_3$) was transfected into AH1c cells. Following 3 weeks of culturing in the presence of G418, more than 10 colonies were obtained, and then 8 colonies (#2, #3, #4, #5, #6, #8, #13, and #14) were successfully proliferated. We initially selected colonies #2, #3, and #14 because they had high levels of RL activity ($>4 \times 10^6$ U/1.6×10^5 cells) (Fig. 1a). However, RT-PCR and the sequencing analyses revealed that the genome-length HCV-AH1 RNAs obtained from these colonies each had an approximately 1 kb deletion in the E2 region (data not shown). In this regard, we previously observed similar phenomenon and described the difficulty of the development of a luciferase reporter assay system using the genome-length HCV RNA of more than 12 kb [7], suggesting that the NS5B polymerase possesses the limited elongation ability (probably up to a total length of 12 kb). Indeed, in that study, we could overcome this obstacle by the selection of the colony harboring a complete genome-length HCV RNA among the obtained G418-resistant colonies [7]. Therefore, we next carried out the selection among the other colonies. Fortunately, we found that colony #4, showing a rather high level of RL activity (2×10^6 U/1.6×10^5 cells), possessed a complete genome-length HCV-AH1 RNA without any deleted forms, although most of the other colonies possessed some amounts of a deleted form in addition to a complete genome-length HCV-AH1 RNA (data not shown). We demonstrated that the HCV RNA sequence was not integrated into the genomic DNA in colony #4 (data not shown). From these results, we finally selected colony #4, and it was thereafter referred to as AH1R and used for the following studies.

We first demonstrated that AH1R cells expressed sufficient levels of HCV proteins (Core, E2, and NS5B) by Western blot analysis for the evaluation of anti-HCV reagents, and the expression levels were almost equivalent to those in OR6 cells (Fig. 1b). In this analysis, we confirmed that the size of the E2 protein in AH1R cells was 7 kDa larger than that in OR6 cells (Fig. 1b), as observed previously [12]. This result indicates that AH1R cells express AH1 strain-derived E2 protein possessing two extra N-glycosylation sites [12]. We next demonstrated good correlations between the levels of RL activity and HCV RNA in AH1R cells (Fig. 1c), as we previously demonstrated in OR6 cells treated with IFN-α for 24 h [7]. These correlations indicate that AH1R cells were as useful as OR6 cells as a luciferase assay system.

Aa substitutions detected in genome-length HCV RNA in AH1R cells

To examine whether or not genome-length HCV RNA in AH1R cells possesses additional conserved mutations such as adaptive mutations, we performed a sequence analysis of HCV RNA in AH1R cells. The results (Fig. 2) revealed that

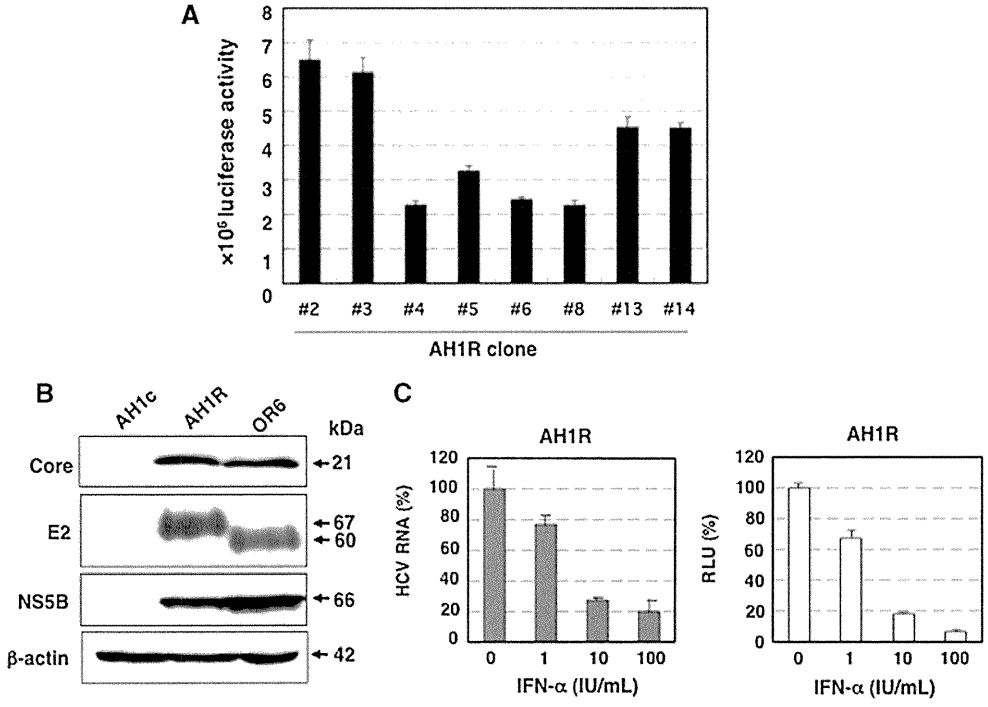

Fig. 1 Characterization of AH1R cells harboring genome-length HCV RNA. **a** Selection of G418-resistant cell clones. The levels of HCV RNA in G418-resistant cells were monitored by RL assay. **b** Western blot analysis. AH1c, AH1R, and OR6 cells were used for the comparison. *Core, E2,* and *NS5B* were detected by Western blot analysis. *β*-actin was used as a control for the amount of protein loaded per lane. **c** RL activity is correlated with HCV RNA level. The AH1R cells were treated with IFN-α (0, 1, 10, and 100 IU/mL) for 24 h, and then a luciferase reporter assay (*right panel*) and quantitative RT-PCR (*left panel*) were performed. The relative luciferase activity (RLU) (%) or HCV RNA (%) calculated at each point, when the level of luciferase activity or HCV RNA in non-treated cells was assigned to be 100%, is presented here

two additional mutations accompanying aa substitutions (W860R (NS2) and A1218E (NS3)) were detected commonly among the three independent clones sequenced, suggesting that these additional mutations are required for the efficient replication or stability of genome-length HCV RNA. The P1115L (NS3), L1262S (NS3), V1897A (NS4B), and V2360A (NS5A) mutations derived from the sAH1 replicon [12] were conserved in AH1R cell-derived clones. However, AH1-clone-2-specific mutations (T1338A and V1880A) were almost reverted to the consensus sequences of AH1 RNA [12] except for V1880A in AH1R clone 2 (Fig. 2). In addition, the Q63R (Core) mutation was observed in two of three clones (Fig. 2).

Comparison between the AH1R and OR6 assay systems regarding the sensitivities to IFN-α, IFN-γ, and CsA

Using quantitative RT-PCR analysis, we previously examined the anti-HCV activities of IFN-α, IFN-γ, and CsA in AH1 and O cells, and noticed different anti-HCV profiles of IFN-γ and CsA between AH1 and O cells [12]. In that study, AH1 cells seemed to be more sensitive than the O cells to CsA (significant difference was observed when 0.063, 0.12, or 0.25 μg/mL of CsA was used). Conversely, AH1 cells seemed to be less sensitive than the O cells to IFN-γ (significant difference was observed when 1 or 10 IU/mL of IFN-γ was used). However, we were not able to determine precisely the EC_{50} values of these reagents, because of the unevenness of the data obtained by RT-PCR.

After developing the AH1R assay system in this study, we determined the EC_{50} values of IFN-α, IFN-γ, and CsA using the AH1R assay and compared the values with those obtained by the OR6 assay. The results revealed that AH1R assay was more sensitive than OR6 assay to IFN-α (EC_{50}; 0.31 IU/mL for AH1R, 0.45 IU/mL for OR6) (Fig. 3a) and CsA (EC_{50}; 0.11 μg/mL for AH1R, 0.42 μg/mL for OR6) (Fig. 3b), and that the OR6 assay was more sensitive than the AH1R assay to IFN-γ (EC_{50}; 0.69 IU/mL for AH1R, 0.28 IU/mL for OR6) (Fig. 3c). Regarding these anti-HCV reagents, the anti-HCV activities observed between the AH1R and OR6 assays differed significantly in all of the concentrations examined (Fig. 3). In addition, regarding these anti-HCV reagents, cell growth was not suppressed within the concentrations used. Regarding IFN-γ and CsA, the present results clearly support those of our previous

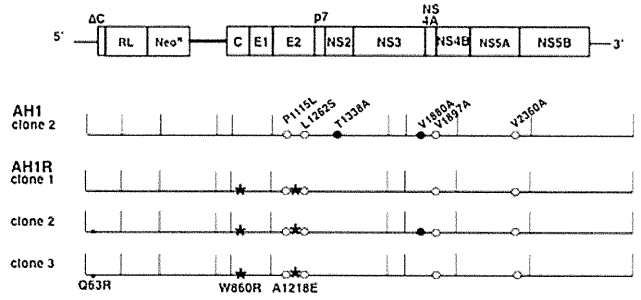

Fig. 2 Aa substitutions detected in intracellular AH1R genome-length HCV RNA. The *upper portion* shows schematic gene organization of genome-length HCV RNA encoding the *RL* gene developed in this study. Genome-length HCV RNA consists of 2 cistrons. In the first cistron, RL is translated as a fusion protein with Neo^R by HCV-IRES, and in the second cistron, all of HCV proteins (C-NS5B) are translated by encephalomyocarditis virus (EMCV)-IRES introduced in the region upstream of C-NS5B regions. Genome-length HCV RNA-replicating cells possess the G418-resistant phenotype because Neo^R is produced by the efficient replication of genome-length HCV RNA. Therefore, when genome-length HCV RNA is excluded from the cells or when its level is decreased, the cells are killed in the presence of G418. In this system, anti-HCV activity is able to evaluate the value of the reporter (RL activity) instead of the quantification of HCV RNA or HCV proteins. In addition, it has been known that the infectious HCV is not produced from this RNA replication system [3, 4, 6]. Core to NS5B regions of three independent clones (*AH1R clones 1–3*) sequenced are presented. W860R and A1218E conserved substitutions are indicated by *asterisks*. Q63R substitutions detected in two of three clones are each indicated by a *small dot*. Core to NS5B regions of *AH1 clone 2*, used to establish the AH1R cell line, are also presented. AH1-specific conserved substitutions and *AH1-clone-2*-specific substitutions are indicated by *open circles* and *black circles*, respectively

study [12]. Therefore, we suggest that the diverse effects of these anti-HCV reagents are due to the difference in HCV strains, although we are not able to completely exclude the possibility that AH1R cells are compromised cells causing the different responses against anti-HCV reagents. In summary, the previous and present findings suggest that the AH1R assay system is also useful for the evaluation of anti-HCV reagents as an independent assay system.

Anti-HCV activity of rolipram was clearly observed in the AH1R assay, but not in the OR6 assay

From the above findings, we supposed that the anti-HCV reagents reported to date might show diverse effects between the drug assay systems derived from the different HCV strains. To test this assumption, we used the AH1R and OR6 assay systems to evaluate the anti-HCV activity of more than 10 pre-existing drugs (6-Azauridine, bisindoly maleimide 1, carvedilol, cehalotaxine, clemizole, 2′-deoxy-5-fluorouridine, esomeprazole, guanazole, hemin, homoharringtonine, methotrexate, nitazoxanide, resveratrol, rolipram, silibinin A, Y27632, etc.), which other groups had evaluated using an assay system derived from the Con1 strain (genotype 1b) or JFH-1 strain (genotype 2a). The results revealed that most of these reagents in the AH1R assay showed similar levels of anti-HCV activities compared with those in the OR6 assay or those of the previous studies (data not shown). However, we found that only rolipram, a selective phosphodiesterase 4 (PDE4) inhibitor [16] that is used as an anti-inflammatory drug, showed moderate anti-HCV activity (EC_{50} 31 μM; $CC_{50} > 200$ μM; $SI > 6$) in the AH1R assay, but no such activity in the OR6 assay (upper panel in Fig. 4a). This remarkable difference was confirmed by Western blot analysis (lower panel in Fig. 4a). It is unlikely that rolipram's anti-HCV activity is due to the inhibition of exogenous RL, Neo^R or encephalomyocarditis virus internal ribosomal entry site (EMCV-IRES), all of which are encoded in the genome-length HCV RNA, because the AH1R and OR6 assay systems possess the same structure of genome-length HCV RNA except for HCV ORF. To demonstrate that rolipram's anti-HCV activity is not due to the clonal specificity of the cells or the specificity of genome-length HCV RNA, we examined the anti-HCV activity of rolipram using the monoclonal HCV replicon RNA-replicating cells (sAH1 cells for AH1 strain [12], and sO cells for O strain [13]). The results

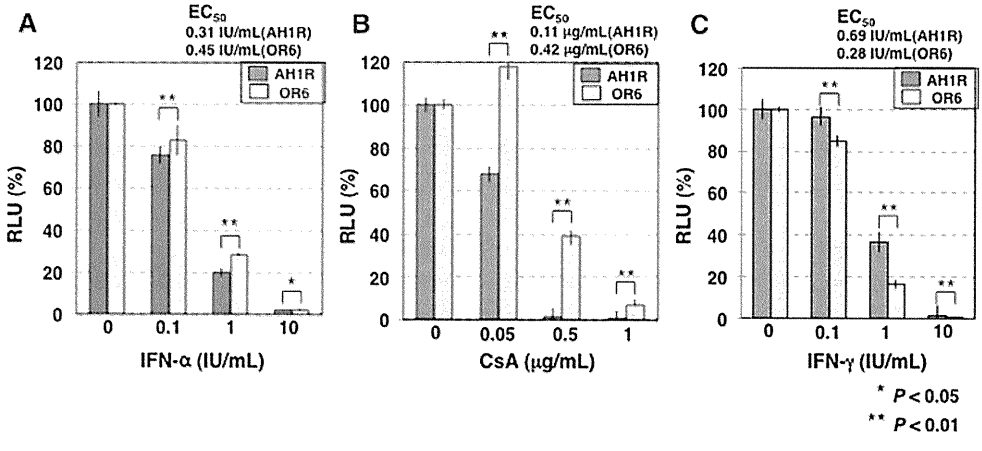

Fig. 3 The diverse effects of anti-HCV reagents on AH1R and OR6 assay systems. AH1R and OR6 cells were treated with anti-HCV reagents for 72 h, and then the RL assay was performed as described in Fig. 1c. **a** Effect of IFN-α. **b** Effect of CsA. **c** Effect of IFN-γ

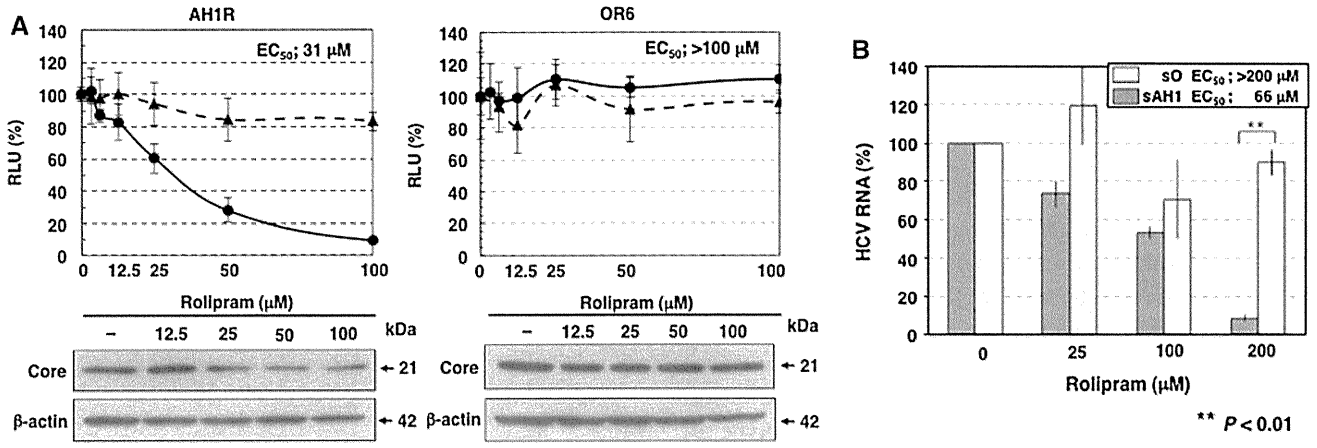

Fig. 4 Anti-HCV activity of rolipram. **a** Rolipram sensitivities on genome-length HCV RNA replication in AH1R and OR6 assay systems. AH1R and OR6 cells were treated with rolipram for 72 h, followed by RL assay (*black circle* with *linear line* in the *upper panels*) and WST-1 assay (*black triangle* with *broken line* in the *upper panels*). The relative value (%) calculated at each point, when the level in non-treated cells was assigned to 100%, is presented here. Western blot analysis of the treated cells for the HCV Core was also performed (*lower panels*). **b** Rolipram sensitivities on HCV replicon RNA replication in sAH1 and sO cells. sAH1 and sO cells were treated with rolipram for 72 h, and extracted total RNAs were subjected to quantitative RT-PCR for HCV 5′ untranslated region as described previously [7]. The HCV RNA (%) calculated at each point, when the level of HCV RNA in non-treated cells was assigned to be 100%, is presented here

revealed by quantitative RT-PCR that rolipram showed moderate anti-HCV activity (EC_{50} 66 μM) in sAH1 cells, but no such activity in sO cells (Fig. 4b). Anti-HCV activity of rolipram in sAH1 cells was a little weaker than that in AH1R cells (Fig. 4b). The similar phenomenon that the anti-HCV activity in genome-length HCV RNA-based reporter assay is stronger than that in HCV subgenomic replicon-based reporter assay was observed regarding other anti-HCV reagents in our previous studies [14, 17, 18]. This result suggests that the anti-HCV activity of rolipram is not either a clone-specific or genome-length HCV RNA-specific phenomenon. In our previous studies also [14, 18], we demonstrated that anti-HCV activities of several reagents including ribavirin and statins were not due to the clonal specificity of the cells. On the other hand, it was recently reported that rolipram did not show anti-HCV activity in the JFH-1 strain-derived assay [19]. Taken together, the previous and present results suggest that rolipram's anti-HCV activity differs depending on the HCV strain. In summary, rolipram was identified as a new anti-HCV candidate using the AH1R assay system.

Discussion

In the present study, we developed for the first time a drug assay system (AH1R), derived from the HCV-AH1 strain (from a patient with acute hepatitis C), in which HCV-AH1 RNA is efficiently replicated. Using this system, we found that rolipram, an anti-inflammatory drug, had potential anti-HCV activity. This potential had not been detected by preexisting assay systems such as OR6, in which HCV-O RNA was derived from an HCV-positive blood donor. Since an HCV replicon harboring the sAH1 cell line, the parent of the AH1R cell line, was obtained from OR6-cured cells [12], the divergence in rolipram's effects between AH1R and OR6 cells is probably attributable to the difference in HCV strains rather than to the difference in cell clones. Indeed, rolipram's anti-HCV activity was not observed in another ORL8 assay system (O strain), which was recently developed using a new hepatoma Li23 cell line (data not shown) [15]. Therefore, we propose that multiple assay systems derived from different HCV strains are required for the discovery of anti-HCV reagents such as rolipram or for the objective evaluation of anti-HCV activity.

Comparative evaluation analysis of anti-HCV activities of IFN-α, IFN-γ, and CsA using AH1-strain-derived AH1R and O-strain-derived OR6 assay systems demonstrated that each of these anti-HCV reagents showed significantly diverse antiviral effects between the two systems. Regarding IFN-γ and CsA, the present results obtained using a luciferase reporter assay fully supported our previous findings [12] using quantitative RT-PCR analysis. However, in the present analysis, we noticed that IFN-α also showed significantly diverse effects (especially at less than 1 IU/mL) between the AH1R and OR6 assays.

The differences in IFN-α sensitivity may be attributable to the difference in aa sequences in the IFN sensitivity-determining region (ISDR; aa 2209-2248 in the HCV-1b genotype), in which aa substitutions correlate well with IFN sensitivity in patients with chronic hepatitis C [20], because the AH1 strain possesses three aa substitutions (T2217A, H2218R, and A2224 V) in ISDR, whereas the O strain possesses no aa substitutions. However, no report has demonstrated the correlation between IFN sensitivity and the substitution numbers in ISDR using the cell culture-based HCV RNA replication system.

Alternatively, Akuta et al. [21] reported that aa substitutions at position 70 and/or position 91 in the HCV Core region of patients infected with the HCV-1b genotype are pretreatment predictors of null virological response (NVR) to pegylated IFN/ribavirin combination therapy. In particular, substitutions of arginine (R) by glutamine (Q) at position 70, and/or leucine (L) by methionine (M) at position 91, were common in NVR. The patients with position-70 substitutions often showed little or no decrease in HCV RNA levels during the early phase of IFN-α treatment [21]. Regarding this point, it is interesting that position 70 in the AH1 strain is R (wild type) and that in the O strain is Q (mutant type), whereas position 91 is L (wild type) in both strains. Therefore, wild-type R in position 70 of the AH1 strain may contribute to the high sensitivity to IFN-α in the AH1R assay. Regarding positions 70 and 91 of the HCV Core, it is noteworthy that, among all of the HCV strains used thus far to develop HCV replicon systems, only the AH1 strain possesses double wild-type aa (data not shown). Therefore, the AH1R assay system may be useful for further study of sensitivity to IFN/ribavirin treatment.

The anti-HCV activity of rolipram, which is currently used as an anti-inflammatory drug, is interesting, although its anti-HCV mechanism is unclear. As a selective PDE4 inhibitor [16], rolipram may attenuate fibroblast activities that can lead to fibrosis and may be particularly effective in the presence of transforming growth factor (TGF)-β1-induced fibroblast stimulation [22]. On the other hand, HCV enhances hepatic fibrosis progression through the generation of reactive oxygen species and the induction of TGF-β1 [23]. Taken together, the previous and present results suggest that rolipram may inhibit both HCV RNA replication and HCV-enhanced hepatic fibrosis. However, it is unclear that rolipram shows anti-HCV activity against the majority of HCV strains, because rolipram has been effective for AH1 strain, but not for O strain. Although rolipram's anti-HCV activity would be HCV-strain-specific, it is not clear which HCV strain is the major type regarding the sensitivity to rolipram. Since developed assay systems using genome-length HCV RNA-replicating cells are limited to several HCV strains including O and AH1 strains to date, further analysis using the assay systems of other HCV strains will be needed to clarify this point.

In this study, we demonstrated that the AH1R assay system, which was for the first time developed using an HCV strain derived from a patient with acute hepatitis C, showed different sensitivities against anti-HCV reagents in comparison with assay systems in current use, such as OR6 assay. Therefore, AH1R assay system would be useful for various HCV studies including the evaluation of anti-HCV reagents and the identification of antiviral targets.

Acknowledgment This study was supported by grants-in-aid for research on hepatitis from the Ministry of Health, Labor, and Welfare of Japan. K. M. was supported by a Research Fellowship for Young Scientists from the Japan Society for the Promotion of Science.

References

1. N. Kato, Acta Med. Okayama **55**, 133–159 (2001)
2. N. Kato, M. Hijikata, Y. Ootsuyama, M. Nakagawa, S. Ohkoshi, T. Sugimura, K. Shimotohno, Proc. Natl. Acad. Sci. USA **87**, 9524–9528 (1990)
3. R. Bartenschlager, S. Sparacio, Virus Res. **127**, 195–207 (2007)
4. D. Moradpour, F. Penin, C.M. Rice, Nat. Rev. Microbiol. **5**, 453–463 (2007)
5. V. Lohmann, F. Korner, J. Koch, U. Herian, L. Theilmann, R. Bartenschlager, Science **285**, 110–113 (1999)
6. M. Ikeda, N. Kato, Adv. Drug Deliv. Rev. **59**, 1277–1289 (2007)
7. M. Ikeda, K. Abe, H. Dansako, T. Nakamura, K. Naka, N. Kato, Biochem. Biophys. Res. Commun. **329**, 1350–1359 (2005)
8. K. Naka, M. Ikeda, K. Abe, H. Dansako, N. Kato, Biochem. Biophys. Res. Commun. **330**, 871–879 (2005)
9. M. Ikeda, K. Abe, M. Yamada, H. Dansako, K. Naka, N. Kato, Hepatology **44**, 117–125 (2006)
10. A. Nozaki, M. Morimoto, M. Kondo, T. Oshima, K. Numata, S. Fujisawa, T. Kaneko, E. Miyajima, S. Morita, K. Mori, M. Ikeda, N. Kato, K. Tanaka, Arch. Virol. **155**, 601–605 (2010)
11. M. Ikeda, Y. Kawai, K. Mori, M. Yano, K. Abe, G. Nishimura, H. Dansako, Y. Ariumi, T. Wakita, K. Yamamoto, N. Kato, Liver Int. **31**, 871–880 (2011)
12. K. Mori, K. Abe, H. Dansako, Y. Ariumi, M. Ikeda, N. Kato, Biochem. Biophys. Res. Commun. **371**, 104–109 (2008)
13. N. Kato, K. Sugiyama, K. Namba, H. Dansako, T. Nakamura, M. Takami, K. Naka, A. Nozaki, K. Shimotohno, Biochem. Biophys. Res. Commun. **306**, 756–766 (2003)
14. K. Mori, M. Ikeda, Y. Ariumi, H. Dansako, T. Wakita, N. Kato, Virus Res. **157**, 61–70 (2011)
15. N. Kato, K. Mori, K. Abe, H. Dansako, M. Kuroki, Y. Ariumi, T. Wakita, M. Ikeda, Virus Res. **146**, 41–50 (2009)
16. S.J. MacKenzie, M.D. Houslay, Biochem. J. **347**, 571–578 (2000)
17. M. Yano, M. Ikeda, K. Abe, H. Dansako, S. Ohkoshi, Y. Aoyagi, N. Kato, Antimicrob. Agents Chemother. **51**, 2016–2027 (2007)
18. G. Nishimura, M. Ikeda, K. Mori, T. Nakazawa, Y. Ariumi, H. Dansako, N. Kato, Antiviral Res. **82**, 42–50 (2009)
19. P. Gastaminza, C. Whitten-Baue, F.V. Chisari, Proc. Natl. Acad. Sci. USA **107**, 291–296 (2010)
20. N. Enomoto, I. Sakuma, Y. Asahina, M. Kurosaki, T. Murakami, C. Yamamoto, Y. Ogura, N. Izumi, F. Marumo, C. Sato, N. Engl. J. Med. **334**, 77–81 (1996)

21. N. Akuta, F. Suzuki, Y. Kawamura, H. Yatsuji, H. Sezaki, Y. Suzuki, T. Hosaka, M. Kobayashi, M. Kobayashi, Y. Arase, K. Ikeda, H. Kumada, J. Med. Virol. **79**, 1686–1695 (2007)
22. S. Togo, X. Liu, X. Wang, Am. J. Physiol. Lung Cell. Mol. Physiol. **296**, L959–L969 (2009)
23. W. Lin, W.L. Tsai, R.X. Shao, G. Wu, L.F. Peng, L.L. Barlow, W.J. Chung, L. Zhang, H. Zhao, J.Y. Jang, R.T. Chung, Gastroenterology **138**, 2509–2518 (2010)

JVI
Journals ASM.org

Origin and Evolution of the Unique Hepatitis C Virus Circulating Recombinant Form 2k/1b

Jayna Raghwani,[a] Xiomara V. Thomas,[b] Sylvie M. Koekkoek,[b] Janke Schinkel,[b] Richard Molenkamp,[b] Thijs J. van de Laar,[c] Yutaka Takebe,[d] Yasuhito Tanaka,[e] Masashi Mizokami,[f] Andrew Rambaut,[a,g] and Oliver G. Pybus[h]

Institute of Evolutionary Biology, University of Edinburgh, Ashworth Laboratories, Edinburgh, United Kingdom[a]; Academic Medical Center, Department of Medical Microbiology, Section of Clinical Virology, Amsterdam, The Netherlands[b]; VU University Medical Centre, Department of Medical Microbiology and Infection Control, Amsterdam, The Netherlands[c]; AIDS Research Center, National Institute of Infectious Diseases, Tokyo, Japan[d]; Department of Virology and Liver Unit, Nagoya City University Graduate School of Medical Sciences, Nagoya, Japan[e]; The Research Center for Hepatitis and Immunology, National Center for Global Health and Medicine, Ichikawa, Japan[f]; Fogarty International Center, National Institutes of Health, Bethesda, Maryland, USA[g]; and Department of Zoology, University of Oxford, Oxford, United Kingdom[h]

Since its initial identification in St. Petersburg, Russia, the recombinant hepatitis C virus (HCV) 2k/1b has been isolated from several countries throughout Eurasia. The 2k/1b strain is the only recombinant HCV to have spread widely, raising questions about the epidemiological background in which it first appeared. In order to further understand the circumstances by which HCV recombinants might be formed and spread, we estimated the date of the recombination event that generated the 2k/1b strain using a Bayesian phylogenetic approach. Our study incorporates newly isolated 2k/1b strains from Amsterdam, The Netherlands, and has employed a hierarchical Bayesian framework to combine information from different genomic regions. We estimate that 2k/1b originated sometime between 1923 and 1956, substantially before the first detection of the strain in 1999. The timescale and the geographic spread of 2k/1b suggest that it originated in the former Soviet Union at about the time that the world's first centralized national blood transfusion and storage service was being established. We also reconstructed the epidemic history of 2k/1b using coalescent theory-based methods, matching patterns previously reported for other epidemic HCV subtypes. This study demonstrates the practicality of jointly estimating dates of recombination from flanking regions of the breakpoint and further illustrates that rare genetic-exchange events can be particularly informative about the underlying epidemiological processes.

Hepatitis C virus (HCV) infection presents a major global health burden, with the WHO estimating that 170 million chronic carriers are at risk of developing severe clinical outcomes such as cirrhosis and hepatic cellular carcinoma (56, 71). The virus belongs to the single-stranded positive-sense RNA virus family *Flaviviridae* and is characterized by considerable genetic diversity. HCV diversity is classified into six main genotypes (genotypes 1 to 6), each of which is further divided into numerous subtypes, and the virus exhibits nucleotide sequence divergences of 30 and 20% at the genotype and subtype levels, respectively (58). The high genomic heterogeneity of HCV is a result of both its high rate of evolution and its long-term association with human populations (60). Although there is no indication for a zoonotic virus reservoir, a related virus has recently been discovered in dogs (22).

The greatest diversity of HCV is found in West and Central Africa and in Southeast Asia, where the virus appears to have persisted endemically for at least several centuries (49, 60). The current distribution of HCV genotypes and subtypes is geographically structured, reflecting differences in the rates and routes of transmission of the various subtypes and genotypes. Epidemic strains, exemplified by subtypes 1a, 1b, and 3a, are characterized by high prevalence, low genetic diversity, and a global distribution and are typically associated with transmission via infected blood products and injecting drug use (IDU) during the 20th century (13, 44–46, 54, 57). In contrast, endemic strains are more spatially restricted but harbor greater genetic diversity than epidemic strains, and it is currently thought that this endemic diversity provided the source of the epidemic strains that constitute the majority of HCV infections worldwide (47, 60).

Recombination is thought to play a comparatively minor role in shaping the genetic diversity of HCV; however, an increasing number of reports suggests that it is not entirely insignificant in HCV evolution. Most notable of these was the initial discovery of a natural recombinant form of HCV circulating in injecting drug users resident in St. Petersburg, Russia (20). This recombinant, labeled 2k/1b, has a 5′ genome region that is most closely related to subtype 2k and a 3′ genome region that is most closely related to the global epidemic subtype 1b, with a single recombination breakpoint located at genomic position 3175 or 3176 in the NS2 gene (20). Since the discovery of 2k/1b, several other studies have reported both inter- and intragenotypic HCV recombinants in natural populations, although the evidence presented for recombination varies in strength; the weakest studies report only discordant genotyping results between genome regions (which could also result from coinfection), whereas the most convincing studies repeatedly sequence the same recombination breakpoint from independent extractions (thereby excluding the possibility of *in vitro* genetic

Received 31 August 2011 **Accepted** 14 November 2011
Published ahead of print 23 November 2011
Address correspondence to Jayna Raghwani, jna.raghwani@gmail.com, or Oliver G. Pybus, oliver.pybus@zoo.ox.ac.uk.
Supplemental material for this article may be found at http://jvi.asm.org/.

doi:10.1128/JVI.06184-11

exchange). Thus far there have been nine descriptions of HCV recombinant forms, although only in six cases have the breakpoints been sequenced (6–8, 19, 28, 29, 42).

Inspection of the recombination breakpoint positions within the HCV genome reveals a difference between inter- and intragenotypic recombinants. Breakpoints in the intrasubtypic recombinants (1a/1c and 1b/1a) are located in the E1/E2 region, while in the intergenotypic recombinants (including 2k/1b), the breakpoints are consistently found in the NS2-NS3 region (8, 19, 28, 29, 39, 42). Interestingly, naturally occurring intergenotypic HCV recombinants have more often than not involved genotype 2 in the 5′ genome region (19, 20, 28, 29, 42). This may reflect some inherent yet unknown biological or ecological properties of this genotype to produce viable recombinant viruses.

Nevertheless, the low rate of discovery of novel recombinant forms suggests that although recombination does occur in HCV, it is an uncommon event, at least in comparison to HIV-1. Indeed, the 2k/1b strain discovered in St. Petersburg is the only known circulating recombinant form (CRF) of HCV and has therefore been designated CRF01_1b2k, following a naming scheme similar to that developed for HIV-1 recombinants (23). A CRF is a recombinant form that is found repeatedly in different patients. Since its discovery, CRF01_1b2k has been isolated from patients in many countries, including Ireland, France, Cyprus, Azerbaijan, Uzbekistan, and Russia (20, 25, 26, 29, 37–39). CRF01_1b2k is the only recombinant strain of HCV to have transmitted widely; therefore, it is important to investigate its genesis and dissemination in order to understand why it might be unique and to evaluate the likelihood that other HCV recombinant forms could increase in prevalence in the future.

Evolutionary analysis of viral genomes using methods based on molecular clocks and coalescent theory has previously proved useful in reconstructing the epidemic history of various HCV strains, including subtypes 1a and 1b worldwide (33, 46) and subtype 1b in Japan (66). Similar analyses of HCV genotype 4 in Egypt have estimated the timescale of the large HCV epidemic in that country and have confirmed its iatrogenic cause (48, 65). Very little is known about the evolutionary history of HCV subtype 2k, most likely because of the lack of sequence data for the strain.

In order to address the lack of information about the epidemiological and transmission history of HCV CRF01_1b2k, we have conducted a comprehensive evolutionary analysis of all available viral genome sequences using a well-established Bayesian framework (11). Since previously published sequence data on CRF01_1b2k are limited, we sought to increase the sample size by isolating and sequencing a panel of new recombinant isolates from patients of Russian origin resident in Amsterdam, The Netherlands.

By combining information from different genomic regions in a single analysis, we provide the first estimate of the date of the recombination event that generated CRF01_1b2k. The date that we obtained considerably predates the discovery of the strain and requires a reevaluation of the circumstances surrounding its origin. This is the first time that a recombination event has been dated for any virus other than HIV-1 (32, 51, 67) or influenza A virus (27). Further, we estimate the CRF's past rate of transmission and its pattern of global geographic spread. To obtain more precise parameter estimates when dating recombination events, we employed a joint phylogenetic approach that improves on methods previously applied to HIV-1 CRFs (51, 67). The methods introduced here should serve as a model for future phylogenetic investigations of genetic-exchange events in RNA virus populations.

MATERIALS AND METHODS

Identification and sequencing of new HCV 2k/1b isolates from Amsterdam. In the course of a study of HCV-infected patients resident in Amsterdam (unpublished data), it was found that HCV genotyping results from the 5′ untranslated and NS5B regions were discordant for 6 (out of 200) patients. Of these, five were male and one was female, and their mean age was 34 years (Table 1). For this study, the 5′-end sequences were not used.

HCV RNA was isolated from 200 μl plasma using the purification method described by Boom et al. (4). cDNA was generated using random hexamer primers as described before (4). The amplification was performed using a conventional PCR with the following cycling conditions: 2 min at 50°C and 10 min at 95°C, followed by 45 cycles, each consisting of 30 s at 95°C, 30 s at 55°C, and 1 min at 72°C. Amplicons were purified from a 1% agarose gel as described by Boom et al. (4). Amplification of a 724-nucleotide (nt) fragment (unpublished data) of the NS5B region was performed as previously described (40). Amplification of core/E1 was performed in a 25-μl volume using HCV1b/2 F (GCGTGAGRGTCCTG GAG) as the forward primer and HCV1b/2 R (TGCCARCARTANGGCY TCAT) (positions 292 to 312; all primer locations are indicated relative to the H77 reference genome) as the reverse primer, using the same amplification conditions mentioned above. Amplicons were also purified from a 1% agarose gel as described by Boom et al. (4). Sequencing was performed using HCV1b/2F seq (CTTCYTACTAGCTCTYTTGTCTT; positions 128 to 112) as the forward sequencing primer and HCV1b/2R seq (TGCCAACTGCCRTTGGTGT; positions 2386 to 2410) as the reverse sequencing primer.

To confirm that the viral variants were recombinants, a 234-nt fragment harboring the known breakpoint in NS2 was also amplified and sequenced. Amplification and sequencing of the NS2 breakpoint were performed using HCV2K_F (GCACGCCATACTTCGTCAGAG) as the forward primer and HCV1B_R (CAGGTAATGATCTTGGTCTCCA TGT) as the reverse primer, also using the same cycling conditions mentioned above.

In addition to new CRF01_1b2k sequences from Amsterdam, 6 recombinant isolates from an unpublished study were also included. These sequences were sampled from IDUs in Azerbaijan (Table 1). Most of the remaining CRF01_1b2k isolates came from a study of IDUs in Uzbekistan (25) and from a cohort study of HCV-positive patients from seven countries (26); detailed demographic information on isolates from these two studies is provided here (Table 1). In the latter study, all individuals infected with CRF01_1b2k came from either Russia or Uzbekistan, and 6 of these patients were linked to high-risk groups, namely, blood transfusion recipients or intravenous drug users.

Collation of HCV sequence alignments. To investigate the evolutionary origin and spread of HCV CRF01_1b2k, a data set comprising all subtype 2k/1b ($n = 27$), 2k ($n = 15$), and 1b ($n = 71$) isolates for which both core/E1 and NS5B sequences were available was collated from GenBank and the HCV Sequence Database (24) (see Table S1 in the supplemental material). This collection included the 6 newly sequenced isolates obtained from HCV patients in Amsterdam (see above). Alignments for both genome regions were constructed manually, and each alignment contained exactly the same set of taxa. The date and sampling location of each sequence were obtained from the literature or via personal communication (Table 1).

Estimation of genome region-specific rates of evolution. The evolutionary rates of the core/E1 and NS5B regions used in this study could not be estimated directly from our data, because the sample size and range of sample dates were not large or wide enough. In line with previous studies of HCV epidemic history (e.g., see reference 48), we employed an independent data set with significant temporal information to provide the

TABLE 1 Epidemiological and sequence information of the CRF01_1b2k isolates used in this study[a]

Isolate name	Age (yr)	Gender	Sampling location	Risk factor(s)	Country of origin	GenBank accession no.		NS2 breakpoint	Reference or source
						NS5B	Core/E1 accession		
1b2k_AZ_01AZ051_2000	34	M	Azerbaijan	IDU	Azerbaijan	FJ435529	FJ435462	NA	Unpublished
1b2k_AZ_01AZ082_2000	38	M	Azerbaijan	IDU	Azerbaijan	FJ435544	FJ435480	NA	Unpublished
1b2k_AZ_02AZ105_2001	32	M	Azerbaijan	IDU	Azerbaijan	FJ435550	FJ435490	NA	Unpublished
1b2k_AZ_02AZ114_2001	41	M	Azerbaijan	IDU	Azerbaijan	FJ435556	FJ435497	NA	Unpublished
1b2k_AZ_02AZ129_2001	30	M	Azerbaijan	IDU	Azerbaijan	FJ435564	FJ435505	NA	Unpublished
1b2k_AZ_02AZ139_2001	33	M	Azerbaijan	IDU	Azerbaijan	FJ435572	FJ435514	NA	Unpublished
1b2k_CY_CYHCV037_2005	NA	NA	Cyprus	ST/IDU	Georgia	EU684614	EU684686	NA	9
1b2k_CY_CYHCV093_2007	NA	NA	Cyprus	ST/IDU	Georgia	EU684649	EU684728	NA	9
1b2k_AM_P077_2006	35	M	Amsterdam	IDU	Russia	JF949902	JF949908	Confirmed	This study
1b2k_AM_P079_2006	42	M	Amsterdam	NA	Georgia	JF949897	JF949903	Confirmed	This study
1b2k_AM_P108_2007	35	M	Amsterdam	IDU	Georgia	JF949898	JF949904	Confirmed	This study
1b2k_AM_P135_2005	35	F	Amsterdam	NA	Georgia	JF949899	JF949905	Confirmed	This study
1b2k_AM_P159_2007	39	M	Amsterdam	NA	Georgia	JF949900	JF949906	Confirmed	This study
1b2k_AM_P179_2000	21	M	Amsterdam	IDU	Georgia	JF949901	JF949907	Confirmed	This study
1b2k_FR_M21_2007	30	M	France	IDU	Georgia	FJ821465	FJ821465	Confirmed	38
1b2k_IE_HC9A99966_2006	NA	NA	Ireland	NA	Russia	AB327058	AB327018	Confirmed	37
1b2k_RU_747_1999	NA	NA	Russia	IDU	Russia	AF388411	AY070214	Confirmed	20, 21
1b2k_RU_796_1999	NA	NA	Russia	NA	Russia	AF388412	AY070215	Confirmed	20, 21
1b2k_RU_ALT30_2000	34	F	Russia	NA	Russia	AB327055	AB327015	Confirmed	26
1b2k_RU_HIA1002_2003	NA	NA	Russia	NA	Russia	DQ001221	AB327011	Confirmed	26
1b2k_RU_KNG318_2002	30	M	Russia	IDU	Russia	AY764172	AB327010	Confirmed	26
1b2k_RU_KNG327_2002	25	M	Russia	NA	Russia	AY764176	AB327012	Confirmed	26
1b2k_RU_N687_1999	NA	NA	Russia	NA	Russia	AY587845	AY587845	Confirmed	26
1b2k_RU_PSA108_2005	37	M	Russia	NA	Russia	AB327053	AB327013	Confirmed	26
1b2k_RU_PSA62_2005	50	M	Russia	BT	Russia	AB327054	AB327014	Confirmed	26
1b2k_UZ_AZ15	22	M	Uzbekistan	BT/IDU	Uzbekistan	AB327056	AB327016	Confirmed	25
1b2k_UZ_UZIDU19_2006	NA	NA	Uzbekistan	IDU	Uzbekistan	AB327120	AB327122	Confirmed	25

[a] M, male; F, female; NA, not available; IDU, intravenous drug usage; BT, blood transfusion; ST, sexual transmission.

substitution rates of the subgenomic regions of interest. Specifically, we used the data and analysis strategy of a recent study that reported rates of evolution for all HCV genome regions for subtypes 1a and 1b (14). That study utilized an alignment-partition approach, which was implemented in the BEAST program, to estimate region-specific rates (11). We applied a codon-structured nucleotide substitution model (55), an uncorrelated relaxed lognormal molecular clock (10), and a Bayesian skyline coalescent model (12) to both subtype 1a and 1b whole-genome alignments, from which we obtained rate estimates for the precise subgenomic regions (core/E1 and NS5B) used in our analysis of CRF01_1b2k. The Markov chain Monte Carlo chains (MCMCs) were run for 200 million generations and sampled regularly to yield a posterior tree distribution based upon 10,000 estimates. For further analysis details, see reference 14.

Phylogenetic analysis. Preliminary phylogenetic analyses were undertaken to confirm that CRF01_1b2k originated from a single recombination event. Neighbor-joining (NJ) trees of the core/E1 and NS5B data sets were estimated using the PAUP* program (64) with an HKY85 nucleotide substitution model and a gamma distributed among site rate heterogeneity (data not shown).

Next, in order to directly test the hypothesis of a single recombinant origin, we performed Bayesian MCMC analysis of the core/E1 and NS5B data sets in two ways: (i) we constrained the CRF01_1b2k isolates to be a monophyletic clade, and (ii) no phylogenetic constraints were imposed. The hypothesis of a single origin was then tested by performing a Bayes factor (BF) comparison of the marginal likelihoods (41, 63) obtained from these two analyses. This revealed an insignificant difference between the two competing hypotheses; thus, a single recombination event was assumed in following analyses.

Molecular clock analysis. In order to estimate the date of the recombination event that formed CRF01_1b2k, we created separate data sets for the core/E1 and NS5B regions that contained the CRF isolates, plus all available closely related parental subtype reference sequences (belonging to subtype 2k for the core/E1 region and to subtype 1b for the NS5B region). A hierarchical phylogenetic model (62) was used to combine both data sets and thereby provide a joint estimate of the time to the most recent common ancestor (TMRCA) of the CRF clade, while accounting for uncertainty in both genome regions.

As the CRF clade in the different genome regions is known to represent a common evolutionary history, jointly estimating the age of this clade will maximize the explanatory power of the data (62) and is thus more powerful than analyzing the regions independently, as has been done previously (e.g., see reference 67). However, due to the recombination of the different subtypes, we cannot simply assume that a single tree represents the entire genome. Instead, we allow independent trees for each genomic region but maintain the TMRCA of the CRF clade in each region to lie within a small time of each other, while estimating the mean of these as the parameter of interest.

Specifically, separate phylogenies, molecular clock models, and substitution models were estimated for the core/E1 and NS5B regions. The genome region-specific rates (estimated as described above) were used as prior distributions for the evolutionary rates for the core/E1 and NS5B regions. For the NS5B region, the rates estimated from subtype 1b were applied, while for the core/E1 region, the average of the 1a and 1b rates was used (because a subtype 2k-specific rate was not available).

For each pair of sampled phylogenies (core/E1 and NS5B) in the posterior distribution of the MCMC, three node dates were obtained (as labeled in Fig. 2): A, the joint TMRCA of the CRF clade; B, the date of the parental node of the CRF clade in the core/E1 subtype 2k phylogeny; and C, the date of the parental node of the CRF clade in the NS5B subtype 1b phylogeny. The former date, together with the more recent of the last two

TABLE 2 Evolutionary rate estimates of the genomic regions used in this study

Genomic region	No. of substitutions/site/yr (10^{-3})[a]		
	HCV subtype 1a	HCV subtype 1b	Average rate
Core/E1	1.75 (1.41, 2.10)	1.36 (1.01, 1.76)	1.56 (1.21, 1.93)
NS5B	0.89 (0.71, 1.07)	0.91 (0.68, 1.14)	0.90 (0.70, 1.11)

[a] The estimates were obtained from HCV subtype 1a and 1b whole genomes using a genomic partition model (see Materials and Methods). The numbers inside parentheses represents the 95% highest posterior density credibility interval.

dates, therefore defines a time range during which the recombination event must have occurred (see Fig. 2). The posterior distribution of this time range was then compiled by repeating the above-described procedure for each pair of phylogenies in the MCMC output. The BEAST analysis model settings were the same as those outlined in the section on genome region-specific rates above.

CRF01_1b2k transmission history. Further Bayesian MCMC phylogenetic analyses were performed solely on the CRF01_1b2k isolates in order to estimate the epidemic history and basic reproductive number, R_0, of the strain since its emergence. BEAST model settings were the same as those outlined above, except that different coalescent models were employed to reconstruct the transmission history of the CRF. Both the GMRF skyride (36) and exponential-growth coalescent models were used.

RESULTS

Estimation of genome region-specific rates of evolution. The rates of evolution of the core/E1 and NS5B genomic regions used in this study were estimated from subtype 1a and 1b whole-genome data sets (see Materials and Methods) and are given in Table 2. The rates for the NS5B region corresponded between subtypes, with similar 95% highest posterior density (HPD) intervals, while the rate estimates for the core/E1 region did show some variation among subtypes (Table 2).

Phylogenetic analysis. To establish the evolutionary origins of the HCV 2k/1b strain, we analyzed the core/E1 (644 nt) and NS5B (741 nt) regions of 27 CRF 1b/2k, 15 subtype 2k, and 71 subtype 1b isolates. The 2k/1b isolates were sampled between 1999 and 2007 and were from the following locations: Ireland, Uzbekistan, Azerbaijan, Cyprus, Amsterdam, France, and Russia (Table 1). Since the BF test supported the hypothesis that the 2k/1b isolates were monophyletic, a single origin of the CRF was inferred (BFs for the comparisons of monophyly and nonmonophyly models were 0.31 for the core/E1 data set and −0.68 for the NS5B data set). Furthermore, the monophyletic origin of the CRF clade was supported in both genome regions when no phylogenetic constraints were imposed. However, monophyly of CRF 1b/2k isolates was not supported by a high posterior probability (0.67) in the NS5B maximum clade credibility (MCC) tree, most likely reflecting the uncertainty associated with the star-like phylogeny and relatively short sequence length. However, the recombinant nature of many of the isolates in this study was confirmed by direct observation of the breakpoint in the NS2 gene region (confirmed isolates are represented by filled circles in Fig. 1).

Molecular clock analysis. Figure 1 and Table 3 provide the estimated TMRCAs of the CRF clade obtained using the joint and independent molecular clock analyses. The estimates obtained separately from the core/E1 and NS5B data sets were in close agreement and exhibit overlapping 95% HPD intervals. These estimates also agree with the joint estimate of TMRCA of the CRF (node A), which was 1946 (1932 to 1959; Table 3). We also estimated the date of the most recent common ancestor of the CRF clade and its most closely related parental isolate (Fig. 2). These estimates were again similar for both genome regions, at about 1933 (Table 3). Lastly, by comparing the HPDs of the node A date with the dates of the more recent of the two parental nodes (either B or C), we were able to generate bounds for the time of the

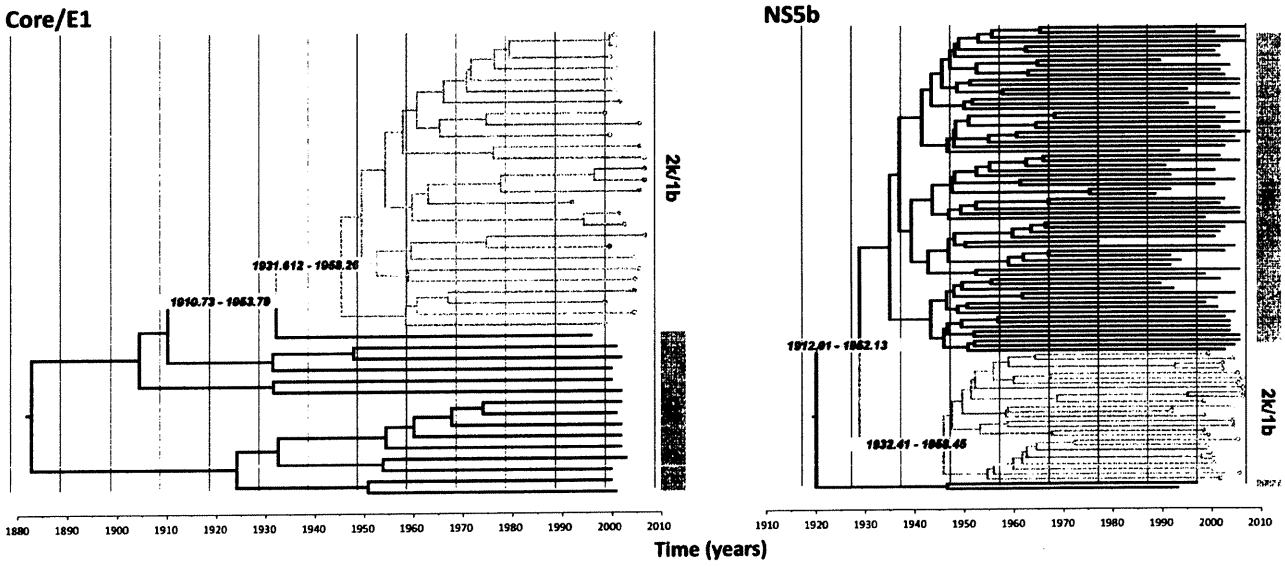

FIG 1 Molecular clock phylogenies of CRF01_1b2k and its parental subtypes, estimated from the core/E1 alignment and the NS5B alignment. The horizontal bars in each phylogeny contain the dating estimates for two nodes: the common ancestor of the CRF clade (1931 or 1932 to 1958) and the common ancestor of the CRF and the most closely related parental strain (1910 to 1912 to 1952 or 1953). Filled circles, 2k/1b isolates that were confirmed as being recombinant by sequencing of the breakpoint in the NS2 region; open circles, those isolates for which NS2 sequences were not available. The trees shown are the maximum clade credibility trees from the Bayesian MCMC analysis.

TABLE 3 Estimates of TMRCA of the CRF clade obtained from separate genome regions and from joint (hierarchical) phylogenetic analysis

Clade (node[a])	TMRCA (yr)[b]		
	Core/E1	NS5B	Joint (hierarchical) estimate
CRF (A)	1945.2 (1931.6, 1958.3)	1945.8 (1932.4, 1958.5)	1946.0 (1932.5, 1959.0)
CRF + 2k (B)	1932.0 (1909.7, 1952.8)	NA	NA
CRF + 1b (C)	NA	1933.1 (1912.0, 1952.1)	NA

[a] The node labels highlighted in Fig. 2.
[b] The numbers inside parentheses represent the 95% highest posterior density credibility interval. NA, not available.

recombination event that generated the CRF, which was between 1923 and 1956.

CRF01_1b2k transmission history. Figure 3 shows the estimated epidemic history of CRF01_1b2k, as estimated using the Bayesian skyride plot method, which depicts the effective population size of the CRF epidemic over time. The plot indicates approximately constant exponential growth since the emergence of the CRF lineage (Fig. 3) until the mid-1990s, after which the effective population size declines or stabilizes (either is plausible, given the size of the credible region of the estimate). This decrease/stabilization coincides with the advent of screening for HCV in blood donors, which greatly reduced the risk of HCV infection via blood transfusion (31, 52, 70).

To ascertain the CRF's exponential growth rate (r), the CRF data set was also analyzed using an exponential-growth coalescent model. The estimated growth rate was 0.116 year^{-1} (95% HPD interval, 0.079 to 0.159). This estimate was subsequently used to calculate R_0 values for the CRF01_1b2k strain under a plausible range of average durations of infectiousness (D), using the equation $R_0 = rD + 1$ (46). Both the estimated growth rate (r = 0.1 year^{-1}) and the estimated R_0 values (R_0, ~2 to 4) are compatible with a number of equivalent estimates for other HCV subtypes, including those from IDU risk groups (46–48, 66).

The MCC tree of the CRF01_1b2k clade (Fig. 4), when combined with all available epidemiological information (Table 1), indicates a clear pattern of phylogenetic clustering according to the geographic location and risk factor of each patient. For example, where these details were available, 14 out of 15 isolates were associated with IDU, while only 1 was isolated from a patient with a history of blood transfusion (Table 1). These observations further support the view that CRF01_1b2k transmission is strongly linked with the IDU transmission route. Although it is not possible to reconstruct the location of the common ancestor of the CRF lineage with any certainty (because our sample size is small and the basal branches of the phylogeny are poorly supported), all of the isolates included in this study are from or have an epidemiological link to the former Soviet Union, and the oldest strain was sampled in Russia in 1999. A well-supported cluster of strains from Azerbaijan originated in about 1970, and therefore, the CRF has likely circulated there since that time. Hence, it appears that CRF01_1b2k disseminated throughout the Soviet Union before its dissolution in the late 1980s and for some time prior to the discovery of the CRF in St. Petersburg in 1999.

DISCUSSION

As the only known HCV recombinant in widespread circulation, the existence and emergence of CRF01_1b2k present an interesting question in HCV epidemiology and evolution. Investigating its evolutionary origins and transmission history helps to understand the circumstances that led to its unique properties. In contrast to HIV, which has 49 known CRFs and a much greater number of unique recombinant forms (30), recombination typically contributes little to the generation and maintenance of HCV genetic diversity. Given that HCV has a higher global prevalence than HIV and, thus, all else being equal, there is a high likelihood of dual infections with divergent HCV strains, it is unlikely that epidemiological factors are

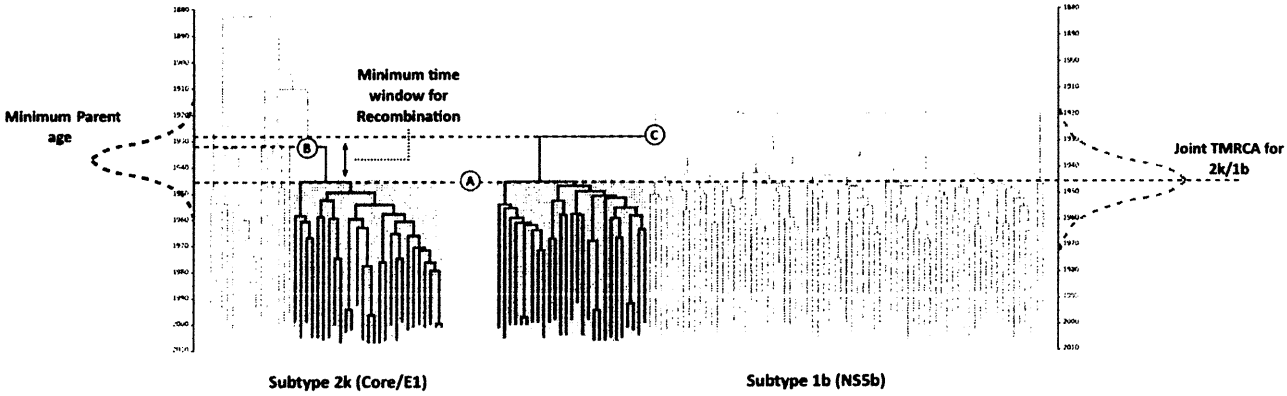

FIG 2 An illustration to explain the structure of the joint phylogenetic method that we employed to estimate the date of the recombination event that generated CRF01_1b2k. The core/E1 tree is shown on the left and the NS5b tree on the right; in both, the shaded box highlights the CRF01_1b2k clade. The left axis depicts the time of the ancestral nodes (node B in the core/E1 tree and node C in the NS5B tree). The right axis shows the TMRCA of CRF01_1b2k (node A). Both CRF node A (estimated jointly from the core/E1 and NS5B regions) and the youngest parental node (either B or C) were used to calculate the minimum time window for the recombination event to have occurred.